Julia Sophie Schartner, BSc

Airspace Limitation for UAV using GNSS

MASTER'S THESIS

to achieve the university degree of

Diplom-Ingenieurin

(Master of Science)

Master's degree program: Geomatics Science

submitted to

Graz University of Technology

Supervisor

Univ.-Prof. Dipl.-Ing. Dr.techn. Dr.h.c.mult. Bernhard Hofmann-Wellenhof

Institute of Geodesy

Co-supervisor

Dipl.-Ing. Dr.techn. Philipp Berglez

Graz, January 2018

Affidavit

I declare that I have authored this thesis independently, that I have not used other than the declared sources/resources, and that I have explicitly indicated all material which has been quoted either literally or by content from the sources used.
The text document uploaded to TUGRAZonline is identical to the present master's thesis.

Graz, _____ _____

Date Signature

Eidesstattliche Erklärung

Ich erkläre an Eides statt, dass ich die vorliegende Arbeit selbstständig verfasst, andere als die angegebenen Quellen/Hilfsmittel nicht benutzt, und die den benutzten Quellen wörtlich und inhaltlich entnommenen Stellen als solche kenntlich gemacht habe.
Das in TUGRAZonline hochgeladene Textdokument ist mit der vorliegenden Masterarbeit identisch.

Graz, am _____ _____

Datum Unterschrift

Acknowledgments

Writing these acknowledgments means I have actually finished this thesis. It means I made it! However, this would not have been possible without the support of so many people, and for that I am very grateful. Thank you for being my motivation and support system!

I want to thank my supervisors, Prof. Bernhard Hofmann-Wellenhof and Philipp Berglez, for their guidance, for supporting my ideas and offering suggestions to help me along the way. I want to thank my colleagues at TeleConsult Austria, who were always willing to help me, even when it meant having lots of patience. Thank you!
I want to thank my friends for forgiving me for being antisocial during the last months and for understanding this situation would not last forever. I want to thank everybody who used their spare time for proofreading this thesis – particularly Sophie, who never seemed to mind the work. Thank you!
I want to thank my parents for offering me wise counsel when needed and for their everlasting support and understanding. Without them I would not be where I am today. And I want to thank Roman for sticking with me when I was freaking out, for motivating me when it seemed impossible and for reminding me there are other things besides work. Thank you!

Julia Schartner

Abstract

In Austria operations of unmanned aerial vehicles (UAVs) are only regulated for the usage within the visual line of sight (Class 1 in § 24f Luftfahrtgesetz) and only up to a maximum altitude of 150 m above ground. Operations beyond visual line of sight (BVLOS) (Class 2 in § 24g Luftfahrtgesetz), however, are neither regulated by the Austrian aviation law nor by the standards and recommended practices (SARPs) from the International Civil Aviation Organization (ICAO). Therefore, operational and technical guidelines for the operation beyond visual line of sight are attained within the research project "Demonstration of UAS Integration for VLL Airspace Operations (DEMONA)". These guidelines include a reference architecture for the UAV and the ground control station as well as the navigation performance.

This thesis deals with the limitation of the flight path using Global Navigation Satellite Systems (GNSS) for positioning. The main focus lies on ensuring that the UAV is not leaving the designated airspace. For this purpose, the position solution is continually covered by a safety envelope including protection levels and the dimensions of the UAV. To determine whether the drone is located inside or outside the protected airspace, its position is intersected with the borders of the defined airspace. In addition, the position is predicted into the future using a Kalman filter. This provides enough time for the pilot to react in case the UAV leaves the defined corridor while maintaining current heading and motion. First data sets were retrieved from a test flight with an ultra light aircraft. Tests are promising a reliable airspace separation by the applied algorithm.

Kurzfassung

Der Betrieb von unbemannten Luftfahrzeugen ist in Österreich nur für den Einsatz im unmittelbaren Sichtbereich des Benutzers am Boden (Klasse 1 gem. § 24f Luftfahrtgesetz) und nur bis zu einer maximalen Flughöhe von 150 m über Grund geregelt. Hinsichtlich des Betriebs außerhalb der Sichtweite (BVLOS) des Piloten (Klasse 2 gem. § 24g Luftfahrtgesetz) gibt es derzeit weder Vorschriften im österreichischen Luftfahrtgesetz noch Standards und empfohlene Praktiken (SARPs) seitens der International Civil Aviation Organization (ICAO). Im Rahmen des Forschungsprojekts „Demonstration of UAS Integration for VLL Airspace Operations (DEMONA)“ werden deshalb operationelle und technische Rahmenbedingungen für einen Einsatz außerhalb des visuellen Sichtbereichs erarbeitet. Diese beinhalten neben einer Referenzarchitektur für das unbemannte Luftfahrzeug und Bodenkontrollstation auch die Navigationsanforderungen.

Die vorliegende Diplomarbeit beschäftigt sich mit der Abgrenzung des Flugpfades mittels Positionierung über globale Satellitennavigationssysteme (GNSS). Der Fokus liegt dabei auf der Sicherstellung, dass der abgegrenzte Luftraum nicht verlassen wird. Hierfür werden die Positionslösungen kontinuierlich um eine Sicherheitsumhüllende, bestehend aus Protection Levels und den Dimensionen des unbemannten Luftfahrzeugs, erweitert. Zur Feststellung, ob sich die Drohne noch innerhalb des definierten Luftraumes befindet, werden dessen Grenzen mit der Position des unbemannten Luftfahrzeugs geschnitten. Zusätzlich wird die zukünftige Position mittels eines Kalman Filters in die Zukunft prädiziert. Dies soll dem Piloten ausreichend Zeit zum Reagieren geben, gesetzt dem Fall, dass das

unbemannte Luftfahrzeug den vorgegebenen Korridor, unter Beibehaltung des aktuellen Kurses und Bewegung, verlässt. Erste Datensätze lieferte ein Testflug mit einem Ultraleichtflugzeug. Tests zeigen, dass eine verlässliche Luftraumabgrenzung mit dem zugrunde liegenden Algorithmus möglich ist.

Contents

Abbreviations

ATC	Air traffic control
ATM	Air traffic management
BLUE	Best linear unbiased estimate
BMVIT	Bundesministerium für Verkehr, Innovation und Technologie (Federal Ministry for Transport, Innovation and Technology)
BRLOS	Beyond radio line of sight
BVLOS	Beyond visual line of sight
C/A	Coarse/acquisition
C/N0	Carrier-to noise power density ratio
DEMONA	Demonstration of UAS Integration for VLL Airspace Operations
EASA	European Aviation Safety Agency
ECEF	Earth-centered, earth-fixed
EDAS	EGNOS Data Access Service
EGNOS	European geostationary navigation overlay service
ESA	European Space Agency
EU	European Union
FEC	Forward error correction
FFG	Österreichische Forschungsförderungsgemeinschaft (Austrian Research Promotion Agency)
FMS	Flight management system
GAGAN	GPS-aided and geoaugmented navigation

Abbreviations

GBAS	Ground-based augmentation system
GIVE	Grid ionospheric vertical error
GGTO	GPS to Galileo time offset
GLONASS	Global'naya Navigatsionnaya Sputnikovaya Sistema (Global Navigation Satellite System)
GNSS	Global navigation satellite system
GPS	Global Positioning System
GPST	GPS time
GSA	European GNSS Agency
GST	Galileo system time
GTRF	Galileo terrestrial reference frame
HDOP	Horizontal dilution of precision
ICAO	International Civil Aviation Organization
IGP	Ionospheric grid point
IMU	Inertial measurement unit
IOC	Initial operational capability
IPP	Ionospheric pierce point
IRNSS	Indian Regional Navigation Satellite System
ISPA	International Symposium on Precision Approach and Performance Based Navigation
ITRF	International Terrestrial Reference Frame
ITRS	International Terrestrial Reference System
JARUS	Joint Authorities for Rulemaking on Unmanned Systems
LBS	Location-based service
MEO	Medium earth orbit
MSAS	MTSAT space-based augmentation system
MTSAT	Multifunctional transport satellite
PBN	Performance based navigation

Abbreviations

PDOP	Position dilution of precision
PRN	Pseudorandom noise
QZSS	Quasi-Zenith Satellite Systems
RPA	Remotely piloted aircraft
RPAS	Remotely piloted aircraft system
RNAV	Area navigation
RSS	Root sum square
RTCA	Radio Technical Commission for Aeronautics
SARPs	Standards and recommended practices
SBAS	Space-based augmentation system
SESAR	Single European Sky Air traffic management Research
SISA	Signal-in-space accuracy
SNR	Signal-to-noise ratio
TAI	International atomic time
UAS	Unmanned aerial system
UAV	Unmanned aerial vehicle
UDRE	User differential range estimate
UTC	Universal time coordinated
VDOP	Vertical dilution of precision
VFR	Visual flight rules
VLL	Very low level
WAAS	Wide-area augmentation system
WGS-84	World Geodetic System 1984

1 Introduction

The constantly growing market of unmanned aerial vehicles (UAVs) is having a growing impact – especially on the aviation industry. According to SESAR (2016), the European market alone will exceed 10 billion Euro annually by 2035 and provide approximately 100 000 jobs throughout member states of the European Union (EU). By 2050 there will be around 7 million leisure drones and 400 000 commercially used drones in Europe.
Recent incidents, for example, the endangerment of the Austrian ski racer Marcel Hirscher by a camera drone during a ski race (Die Presse 2015) or more recently the UAV that came dangerously close to an emergency helicopter at Salzburg Airport (Salzburger Nachrichten 2017), are consistently making newspaper headlines. In July 2017, several aircraft had to divert to alternate airports or were put into holding patterns because of a runway closure caused by a drone flying too close to London Gatwick airport (BBC News 2017). The number of applications, in which drones can be used, is also increasing – recent innovations include the Amazon drone delivery system "Amazon Prime Air" (Hern 2016) and a drone that is used to chase burglars (Lossau 2017).
For these reasons, the operation of UAVs requires precise regulation – especially concerning their usage of the airspace. The regulation of camera drones (for example, for mapping or photographing somebody else's property) should also include the law of data protection.
In Austria, UAV are legally divided in two classes:

- Class 1: Operations within line of sight
  (i.e., constant visual contact from the pilot to the UAV)

- Class 2: Operations beyond line of sight
  (i.e., no visual contact from the pilot to the UAV)

Neither International Civil Aviation Organization (ICAO) standards nor regulations on a national level in Austria exist for Class 2. However, there is a strong need to regulate the usage of the airspace by UAV with operations beyond visual line of sight (BVLOS) due to the growing number of UAVs and their applications. The goal of the research project DEMONA is to contribute solutions for operation of UAVs beyond visual line of sight, including the command and control link to the ground control station, collision avoidance and navigation performance. The latter is covered within this thesis by defining a reference flight path and determining if the UAV is still located within the designated airspace and will not leave it for the duration of the flight. A safety envelope is defined based on the dimensions of the UAV together with a statistical bound error for the measure of integrity (protection levels) when using global navigation satellite system (GNSS) for position determination. In the case of Class 2 certified flights, in which the pilot cannot establish visual contact with the UAV, and therefore cannot react accordingly to the situation without technical aids, the pilot will be notified if the drone is about to leave the flight corridor so an appropriate and timely reaction is possible.

1.1 Thesis Outline

Chapter 1 states the motivation for this thesis, which is the research project Demonstration of UAS Integration for VLL Airspace Operations (DEMONA), together with an overview of the current state of technology. Chapter 1 also explains the legal guidelines for UAV operation and provides a classification of UAVs. Chapter 2 gives a short introduction to the basic principles of GNSS and space-based augmentation systems (SBAS). In this thesis, the Global Positioning System (GPS) and Galileo are used for positioning and accuracy. Integrity information is retrieved via the European geostationary navigation

overlay service (EGNOS), so these are explained in more detail.

This thesis examines how the airspace, in which UAVs are allowed to operate, can be limited. Flight paths are defined using waypoints including a corresponding flight corridor, which is described in Chapter 3.

To account for the bound of the maximum possible position error at the receiver protection levels are calculated, which are contributing to the reliability and integrity of the system. Chapter 4 explains how protection levels are calculated and how a safety envelope is set according to the dimensions and the attitude of the UAV.

Chapter 5 deals with the prediction of the future position of a UAV using a Kalman filter. This is used to ensure that a UAV is not leaving the designated airspace (flight corridor) during flight – while maintaining direction, attitude and velocity. Using a linear prediction, the subsequent protection levels are estimated. The deviation between the current and predicted positions to the reference flight path is divided into its horizontal (across track) and vertical (height) components, which are then compared to the maximum allowed values. If they exceed the defined threshold, the pilot will be warned.

In Chapter 6, the described algorithm is tested and validated using test data from a test flight with a manned aircraft, which was equipped with a GNSS receiver and inertial measurement unit (IMU). Conclusions on this thesis and future possibilities on this topic are provided in Chapter 7.

1.2 Related Research Project

The main goal of the research project Demonstration of UAS Integration for VLL Airspace Operations (DEMONA) is to supply an aircraft system as well as the technical and operational framework for a UAV so it is certifiable for Class 2 operations – for which currently no standards and regulations exist. Very low level (VLL) refers to altitudes of up to 500 ft (150 m) above ground level.

In DEMONA, a software-based GNSS receiver, which is able to process both GPS and Galileo signals and is suitable for operating while embedded in a UAV, is developed. The navigation module processes the GNSS measurements and combines them using an extended Kalman filter with measurements from an IMU, magnetometer and barometer. In addition, special instrument flight procedures are developed for unmanned aerial systems (UAS). Because the UAV is supposed to maneuver beyond visual line of sight, it is equipped with an optical anti-collision system to avoid crashes with terrain or other air traffic. In order to transmit control commands, a communication link that works as well with bad or disturbed transmission channels is tested. In the case of a total system failure, a parachute is released to immediately land the UAV safely. This thesis deals with the navigation performance part of DEMONA.

The project DEMONA is managed by the Austrian Research Promotion Agency (FFG) and received funding from the Federal Ministry of Transport, Innovation and Technology (BMVIT) under the program line TAKE OFF. The project is led by the Institute of Aviation at FH Joanneum Graz, together with its partners the Austrian Institute of Technology, Austro Control, Drone Rescue Systems, Institute of Geodesy at Graz University of Technology, Igaspin and TeleConsult Austria.

1.3 State of the Art

Current state of the art technology for UAV flying along a predefined path concerns mostly autonomous vehicles. In DEMONA, the UAV is supposed to be piloted from a remote station beyond visual line of sight – an autopilot function for the UAV as used in autonomous vehicles is not currently planned.

If an autonomous UAV is supposed to follow a predefined flight path, the path planning is essential. Some approaches on automatic path planning algorithms are introduced in Ambrosino et al. (2006) and in Hota and Ghose (2010). Sujit et al. (2014) reviewed pos-

sible algorithms for path following in 3D space. In Eliker et al. (2016), path planning and guidance are implemented in an embedded flight management system (FMS). Osborne and Rysdyk (2005) suggest an algorithm and look-up table for waypoint guidance under the influence of wind. Most studies concerning beyond line-of-sight applications focus on the communication link as discussed in Soares Lira da Silva et al. (2016). In Skinnemoen (2014), live photography and video communication are used to monitor the aircraft in flight.

Perrottet (2017) discusses the integration of UAS into the airspace and proposes that at least larger UAS should be able to perform performance based navigation (PBN). PBN is the ability of an aircraft to perform standard navigation, which also includes area navigation (RNAV), an instrument navigation procedure using waypoints. A FMS should therefore be able to support ARINC 424 path terminators – the industry standard – which is recommended, for example, when a standard holding pattern needs to be performed. GNSS-only navigation is not recommended because of potential GNSS interference like jamming and spoofing, although additional sensors, as for example an IMU, might solve this issue.

In Lin et al. (2017), the crashing probability for UAV is simulated using a predefined airspace separated into zones, for example, a permanent no-fly zone around airports or skyscrapers or separation between certain flying altitudes. Parameters including the wing span, the maximum take-off weight and fuel capacity were also taken into account. According to this analysis, flight paths are defined, i.e., the radius of a clearance area is set depending on the probability of the crash points. The flight path is then planned considering the defined flight corridor and no-fly zones (e.g. high populated areas) so that the safest route for human population on the ground is found.

Single European Sky Air traffic management Research (SESAR) Joint Undertaking is developing a concept called "U-space" (SESAR 2017). Drones should be integrated into the common airspace by providing new services, such as a management system for drone

operations based on air traffic management (ATM), which would include, among others, flight planning and approval as well as tracking. Further services might be capacity management, assistance for conflict detection and integrated interfaces with manned aviation. U-space should provide a framework which supports routine operations. It is proposed that a large number of UAV should operate in all environments. Nevertheless, a fair access for all airspace users must be achieved. U-space will be deployed progressively depending on the development of UAS and the provided services. It is expected that by 2019 the foundation services (electronic registration and identification and geofencing) will have been established.

The German air traffic control (Deutsche Flugsicherung) and Telekom are working together on a project to integrate drones safely into the airspace. Therefore, UAVs are equipped with a newly developed mobile service and GPS-module (Güttel 2017).

In summary, the majority of research papers deals with flight path planning and guidance for autonomous UAV or provide some guidelines on how the national airspace could be shared between UAS and general classified aircrafts. However, no found research papers focus on the navigation performance using GNSS including the usage of protection levels or the prediction of future positions regarding the limitation of the designated airspace.

1.4 Unmanned Aerial Vehicle

The general definition of unmanned aerial vehicle (UAV) is an aircraft with no pilot on board that is instead controlled either via a remote radio-link, called remotely piloted aircraft (RPA), or a computer system with a pre-planned flight path. An unmanned aerial system (UAS) – or the sub-set remotely piloted aircraft system (RPAS) – includes the UAV and all the elements associated with it, such as a command and control link and a ground control station (ICAO 2011). The control of a UAV can either be ground based (constant input from operator) or autonomous (command and control assets on

board). Semi-autonomous UAV use a guidance system but the remote pilot can override the guidance system at any time (Gupta et al. 2013). UAV operation can be within or beyond line of sight – the latter is divided into beyond visual line of sight (BVLOS) and beyond radio line of sight (BRLOS) (ICAO 2015). According to ICAO (2015) unmanned aircraft can be separated into three (overlapping) classes, as can be seen in Figure 1.1.

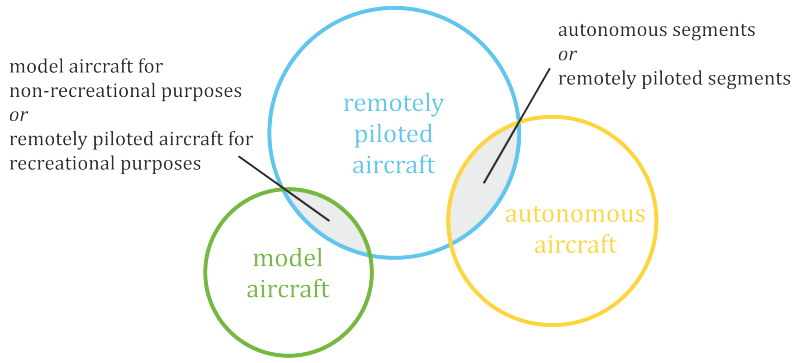

Figure 1.1: Classification of unmanned aircraft

UAVs are used for a variety of applications such as mapping, aerial photography or search and rescue. The fields of application are wide and include the military, agriculture, geodesy, delivery/logistics and meteorological services. Since a UAV is commanded by a remote pilot, the biggest challenge is that the pilot cannot see and react accordingly.
UAV can be organized into four categories depending on the aerodynamic configuration:

- Fixed-wing: unmanned airplanes which require a runway for take-off and landing
- Rotary-wing: advantage of hovering, high maneuverability and vertical take-off different configurations due to placement of rotors, e.g., like a conventional helicopter
- Blimps: lighter than air and long endurance but low speed and usually large, e.g., balloons or airships
- Flapping-wing: flexible wings like birds, mix out of fixed- and rotary-wing possible (hybrids)

UAVs can be also classified according to their endurance, altitude or weight. For example, if a UAV falls in the category *micro*, it is limited to maximum 2 kg and a maximum altitude of 200 ft (approximately 60 m). In the case of DEMONA, it would be a UAV of the category *small*, which weighs between 20 kg and 150 kg and can fly up to 5000 ft (about 1500 km). The maximum radius of mission is unlimited for a *strike/combat* UAV. It weighs up to 600 kg and can reach a maximum altitude of 65 000 ft (around 20 000 m) (Gupta et al. 2013).

1.5 Legal Framework

The legal framework for UAS is not only a national issue but is also handled on an international level. International Civil Aviation Organization (ICAO) is a United Nations specialized agency, which was established in 1944 for the management of administration and governance of civil aviation. As of September 2017, ICAO had 191 member states. The goal is to reach a consensus on international civil aviation standards and recommended practices (SARPs) (ICAO 2017). ICAO is currently working on the integration of RPAS into the airspace, which requires SARPs, procedures and guidance material. ICAO (2015) already provides guidelines on, for example, certification, hazard identification, command and control link and ATC communications.

In Europe, the European Aviation Safety Agency (EASA) was established in 2002 to provide a single regulatory and certification process for its now 32 members, which includes the EU member states as well as Switzerland, Norway, Liechtenstein and Iceland (EASA 2017a). Regulation (EC) No. 216/2008 states that regulations for UAS with more than 150 kg for civil applications do not fall within the competence of the member states of the EU (i.e., national level). EASA (2017b) provides regulations for technical and operational requirements, for example, the identification of drones or geofencing, and classifies UAS

into the three layers of competence (risk categories):

- Open: low risk — maneuver within the visual line of sight up to a maximum altitude in non-restricted areas, no aviation authority needed
- Specific: increased risk — operation authorization needed, e.g., delivery drones
- Certified: high risk — certification of the UAS and licensed remote pilot is needed

The European Commission is contributing to the development of legal guidelines for RPAS, which includes safety, security, privacy and environmental protection (European Commission 2017). In April 2017, an expert group was established to work on further development of legal guidelines. Another contributor on the regional level in Europe is Eurocontrol, an intergovernmental organization with 41 members (Eurocontrol 2017). It provides a road map for safe integration of RPAS into the civil airspace. Eurocontrol and EASA are also members of Joint Authorities for Rulemaking on Unmanned Systems (JARUS).
In Austria the Federal Ministry for Transport, Innovation and Technology (BMVIT) has the supreme authority for civil aviation and it summoned the Austrian Aeroclub (professional association for aviation of non-commercial civil aviation) and Austro Control GmbH (the Austrian air traffic management organization) as secondary aviation authorities (BMVIT 2017). The legal basis for UAV in Austria is the amended aviation law of 2014.

Austrian Aviation Law

For UAV up to 150 kg above the Austrian territory the Austrian Aviation Law[1] is to be applied. The law distinguishes between UAS and model aircraft. The latter are only allowed for recreational activities within a radius of 500 m and always need certification (§ 24c (1) LFG). Certifications for UAV operations in Austria are issued by Austro Control, if the airworthiness requirements are met and there are no safety issues. Special certification

[1] Luftfahrtgesetz (LFG)

is needed if the allowed altitude above ground of 150 m will be exceeded or for flights above large human crowds (for example, open-air concerts or rallies). According to § 24d LFG, unmanned aircraft up to 79 Joule of motion energy are exempt.

Class 1 aircraft (§ 24f (1) LFG) are not to be used for military purposes and a direct (i.e., without technical aids) line of sight must exist at all times. Class 1 is divided into four categories depending on weight and the area of operation, as shown in Table 1.1.

max. take-off weight \ area of operation	I undeveloped	II unpopulated	III populated	IV densely populated
≤ 5 kg	A	A	B	C
≤ 25 kg	A	B	C	D
≤ 150 kg	B	C	D	D

Table 1.1: Categories of Class 1 UAV with respect to area of operation and weight

Depending on the category, the requirements for airworthiness of the UAV range from no special requirements (category A) up to tailored certification specifications (category D), and the technical investigation varies between self declaration to a sample inspection. The Class 1 UAS certification process is very precise, however, similar regulations are lacking for Class 2, where no visual contact between UAS and pilot is required according to § 24g (1) LFG.

There is no law or standard which regulated if and how the position of a UAV is to be determined. One possibility, among others (for example, target tracking with an onboard camera), is the usage of GNSS, which is used in DEMONA.

2 Global Navigation Satellite Systems

"Anytime, everywhere, all-weather" is the basic principle of Global Navigation Satellite Systems (GNSS). When this was made possible in the 1980's by introducing the Global Positioning System (GPS), it was impossible to imagine the influence satellite-based positioning would have on everyday life. Multiple other global systems have developed over the past three decades. Besides the American GPS, there is the Russian Global'naya Navigatsionnaya Sputnikovaya Sistema (GLONASS), the European Galileo and the Chinese Beidou. In addition, space-based augmentation systems and regional systems exist, such as the Quasi-Zenith Satellite Systems (QZSS) in Japan and the Indian Regional Navigation Satellite System (IRNSS).

GNSS meet the requirements to accurately determine position, velocity and time by processing signals from satellites. According to the GNSS Market Report (GSA 2017b) the applications in location-based service (LBS) – the availability of additional information regarding the user's position – and in the road segment together are more than 93 % of the market share. Other applications include surveying (2.6 %), agriculture (1.3 %), aviation (0.7 %) and drones (0.5 %). This means GNSS services are not solely used for navigation, tracking and positioning anymore but also other fields discovered its benefits. For example, there are geodetic applications like structural monitoring, cadastral surveying and mapping plus in agriculture GNSS is used for farm machinery guidance and livestock tracking. GNSS can also be used for civilian protection, for example, disaster monitoring and prediction. It may be used to encrypt data using highly precise time references and

the energy sector uses GNSS for time synchronization. Fleet management of transport vehicles, such as trains, trucks and ships became easier using real-time positioning. In aviation GNSS is used for navigation, in other words routing and guidance, and positioning. When supported with a space-based augmentation system (SBAS) it is also suitable for safety-of-life operations, such as landing an aircraft.

SBAS is regionally limited and serves mainly as an enhancement of GNSS in terms of accuracy and integrity (trusting that the position solution is correct). The European system is called the EGNOS. The wide-area augmentation system (WAAS) supports GPS in North America, the multifunctional transport satellite (MTSAT) space-based augmentation system (MSAS) is used in Japan and the GPS-aided and geoaugmented navigation (GAGAN) is the Indian system, to name a few. The availability of the information provided by ground-based augmentation systems (GBAS) is more likely limited to an area where the service is needed, e.g., in proximity of an airport.

2.1 Principle

Even though today there are multiple systems available the basic principles are the same. The overall system architecture consists of three segments: the space segment which consists of the satellites in orbit, the control segment which is responsible for managing the space segment, such as deployment and maintenance of the satellites as well as tracking and prediction of their positions, and the user segment which covers the user equipment (receiver) either for military or civilian use (Misra and Enge 2001).

2.1.1 Position Determination

Satellite-based positioning describes the determination of a user position using (artificial) satellites. Therefore, satellite positions are generally assumed to be known (or rather computed with the received ephemerides), so the receiver position can be derived using the

ranges and range differences between user and satellite positions.

The principle of satellite-based positioning is shown in Figure 2.1 considering a satellite along its orbit at a given epoch t.

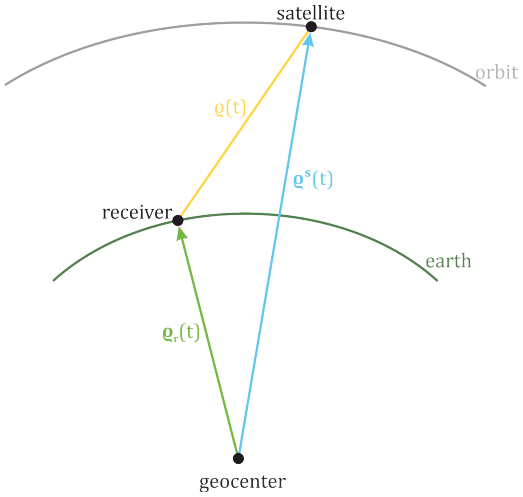

Figure 2.1: Principle of satellite-based positioning

Without considering the possibility of errors caused by imperfect synchronized clocks of receiver and satellite, the receiver position could be calculated using

$$\varrho(t) = \|\boldsymbol{\varrho^s}(t) - \boldsymbol{\varrho_r}(t)\| \ , \tag{2.1}$$

where ϱ equals the geometric range between the satellite and the receiver. Relative to the geocenter are the position vectors of the satellite $\boldsymbol{\varrho^s}$ and the receiver $\boldsymbol{\varrho_r}$ (Hofmann-Wellenhof et al. 2001). The range ϱ is computed by measuring the signal run time Δt between satellite and receiver, which is given by

$$\Delta t = t_r - t^s \ . \tag{2.2}$$

In an ideal case $\varrho = c \cdot \Delta t$ with c being the speed of light. However, satellite and receiver clocks are not synchronized and show biases from the system time (Kaplan et al. 2006). Due to these clock biases the calculated range is denoted as a pseudorange R for a given

epoch t

$$R_r^s(t) = \varrho_r^s(t) + c \cdot \Delta\delta_r^s(t) \ , \tag{2.3}$$

where $\Delta\delta_r^s(t) = \delta_r(t) - \delta^s(t)$ represents the combined clock bias of the receiver and the satellite.

To determine the user position X_r, Y_r, Z_r including the clock bias at least four pseudorange measurements are needed. Each range ϱ between satellite and user defines the surface of a sphere, where the satellite position is at the center. Three satellites are needed to solve for the three unknowns X_r, Y_r, Z_r (components of the position vector $\boldsymbol{\varrho_r}$), assuming a static receiver. The relation can be formed as

$$\varrho_r^s(t) = \sqrt{(X^s(t) - X_r)^2 + (Y^s(t) - Y_r)^2 + (Z^s(t) - Z_r)^2} \ , \tag{2.4}$$

where the components of the space vector $\boldsymbol{\varrho^s}$ are denoted as $X^s(t)$, $Y^s(t)$, $Z^s(t)$ for each epoch t. The fourth measurement is used to determine the unknown clock bias $\Delta\delta_r^s$.

Position accuracy is affected by the accuracy of each satellite's position and pseudorange measurement as well as the geometry of the satellite constellation (Hofmann-Wellenhof et al. 2008) and effects due to the propagation through the ionosphere and troposphere.

2.1.2 Velocity Determination

To determine (radial) velocity using GNSS the approximate derivative of time

$$\dot{\varrho} = \frac{\boldsymbol{\varrho^s} - \boldsymbol{\varrho_r}}{\varrho} \cdot (\dot{\boldsymbol{\varrho}}^{\boldsymbol{s}} - \dot{\boldsymbol{\varrho}}_{\boldsymbol{r}}) = \boldsymbol{\varrho_0} \cdot \Delta\dot{\boldsymbol{\varrho}} \tag{2.5}$$

can be used. This equals geometrically the projection of the relative velocity vector $\Delta\dot{\boldsymbol{\varrho}}$ between satellite and receiver onto the line of sight between satellite and receiver (described as the unit vector $\boldsymbol{\varrho_0}$), as can be seen in Figure 2.2.

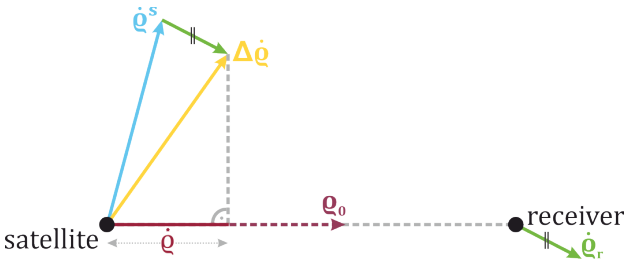

Figure 2.2: Geometrical interpretation of the radial velocity $\dot{\varrho}$

However, a precise estimation of the Doppler frequency can be made with carrier phase measurements. The Doppler principle can be described as the resulting frequency change because of the relative motion of two moving objects, i.e., satellites moving along orbit and a non-static receiver. Because velocity is the differentiation of a range with respect to time the Doppler observable D can be described by the first derivative of the pseudorange, which corresponds to

$$D = \dot{R} = \dot{\varrho} + c \cdot \dot{\delta} \ . \tag{2.6}$$

The resulting Doppler shift Δf arises due to the relative radial motion v_ϱ of the satellite with respect to the user and reads

$$\Delta f = f_r - f^s = -\frac{1}{c} \cdot v_\varrho \cdot f^s \ , \tag{2.7}$$

where f_r is the received frequency and f^s equals the emitted frequency at the satellite (Hofmann-Wellenhof et al. 2008).

2.2 GPS

In 1973 the US Department of Defense directed the Joint Program Office to develop a space-born positioning system which resulted in the present GPS. GPS is a military operated system and its master control station is located at Schriever AFB in Colorado

(Hofmann-Wellenhof et al. 2001). Its alternate master station is located at Vandenberg AFB in California. The ground segment consists of the aforementioned master stations as well as eleven command and control antennas and 16 monitoring sites. The control segment tracks and monitors the GPS satellites.

The space segment of GPS consists of a nominal constellation of 24 satellites with three spares, which is called an "expandable 24"-constellation, in six medium earth orbit (MEO) planes. These planes have a 55° inclination to the equator. The satellites are orbiting in an altitude of approximately 20 200 km and circle the earth approximately every twelve hours. As of 31 August 2017, 31 operational satellites were available for GPS.

Initially GPS used two carrier frequencies (L1: 1575.42 MHz, L2: 1227.60 MHz) for two military signals (P(Y)) and one civilian signal (L1 C/A). During modernization of the satellites – since GPS Block IIR-M in 2005 – a second civilian signal L2C on the L2-carrier is available. With the introduction of the Block IIF satellites in 2010 a third civilian carrier frequency L5 (1176.45 MHz) was established. New Block III satellites are expected in 2018 (at the earliest), which will support a fourth civilian signal L1C on the L1-carrier. This is supposed to enhance the interoperability with other global satellite systems, especially Galileo (U.S. Air Force 2017).

GPS uses the World Geodetic System 1984 (WGS-84) as the terrestrial reference system (details are given in Section 3.1). GPS time (GPST) is a realization of an atomic time system. Synchronization with universal time coordinated (UTC) is achieved by leap seconds. However, GPST itself is not adjusted for leap seconds. This means there is a constant offset to international atomic time (TAI) of 19 seconds. Consequently, the conversion between GPST and UTC varies. In October 2017, the offset was 18 seconds. GPS epochs are counted as GPS weeks and seconds within the current week starting at midnight on Sunday (Hofmann-Wellenhof et al. 2008).

2.3 Galileo

Galileo is Europe's contribution to GNSS. It is supposed to be a civilian system. It is a joint project of the European Commission, the European GNSS Agency (GSA) and the European Space Agency (ESA).

Initial operational capability (IOC) was declared on 15 December 2016, after some difficulties during the deployment phase (for example, satellites launched into a non-nominal orbit in August 2014). The space segment of Galileo is supposed to consist of 24 satellites plus six spares in three circular MEO planes at an altitude of about 23 222 km and an inclination of 56° to the equator (European Union 2016). With this constellation a good coverage up to 75° latitude is ensured. On 12 December 2017, another ARIANE 5 rocket was launched with four Galileo navigation satellites. The system is scheduled to be completed in 2020.

The supported carrier frequencies are listed in Table 2.1. The E1-band supports an interoperability with GPS L1, and E5a and L5 are overlapping. Interoperability with GLONASS G3 is given with the E5b-band (European Union 2016).

Table 2.1: Carrier frequencies transmitted by Galileo

Link	**Frequency** [MHz]	**Wavelength** [cm]
E1	1575.420	19.0
E6	1278.750	23.4
E5	1191.795	25.2
E5a	1176.450	25.2
E5b	1207.140	24.8

The ground segment consists of two Galileo control centers, one in Oberpfaffenhofen (Germany) and one in Fucino (Italy), which process data (for example, integrity information, time synchronization and orbit calculations) provided by a global network of Galileo sensor stations (Falcone et al. 2017).

Galileo will provide five services (Bartolomé et al. 2015):

- Open Service: Open and free of charge for public use
- Commercial Service: Encrypted signal for restricted access for commercial and professional applications
- Public Regulated Service: Restricted signal for governmental usage for sensitive applications
- Search and Rescue: Accurate position information of distress messages (in cooperation with COSPAS-SARSAT)
- Safety-of-Life: Usage for when passenger safety is critical (according to European Commission (2011) not available during IOC)

The used coordinate system is the Galileo terrestrial reference frame (GTRF), which is – as well as WGS-84 – a realization of the International Terrestrial Reference System (ITRS). This supports the interoperability of the systems because the differences between the coordinate systems are supposed to be only a few centimeters.
Galileo system time (GST) is the time system which is referenced to UTC but without using leap seconds and follows with a constant offset TAI. These offsets are broadcasted within the navigation message.
As demonstrated schematically in Figure 2.3, GPST and GST show a small deviation of a few nanoseconds. For distance calculations time is multiplied by the speed of light, so even small differences are not negligible. Therefore, the GPS to Galileo time offset (GGTO) will be distributed via the Galileo or GPS space segment so that combined service is possible (Hofmann-Wellenhof et al. 2008). However, the GGTO can also be estimated as an additional unknown in the position and navigation processing (Conley et al. 2006).

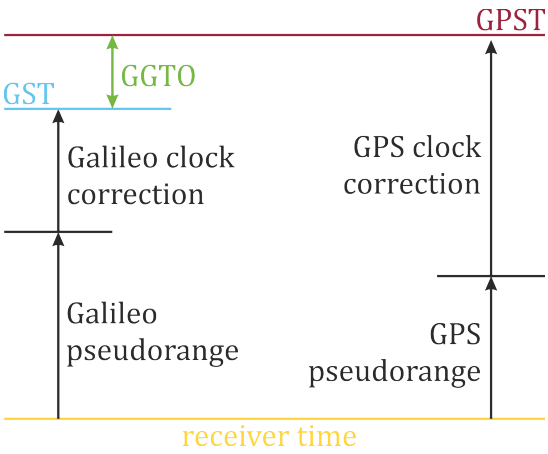

Figure 2.3: Schematic representation of the GGTO with respect to GPST and GST

2.4 Space-based Augmentation Systems

GNSS is not always suitable for applications where (passenger) safety is critical. For example, during critical flight operations in aviation or in maritime harbor maneuvering, it does not meet user requirements for position accuracy and integrity. Therefore, (terrestrial and space-based) augmentation systems, necessary to provide additional information which enhances performance (especially accuracy and integrity), have been developed, e.g., EGNOS, WAAS, GAGAN or MSAS.

SBAS consists of a network of terrestrial monitoring stations which carry out GNSS ranging measurements. The master stations subsequently generate correction parameters for satellite orbits and clocks as well as for ionospheric delays which are then transmitted to the satellite and from there to the user. The space segment consists of at least two geostationary satellites.

Integrity information, enhanced accuracy and increased availability are the three benefits of SBAS. The corrections are broadcasted to the user via a GPS-like signal (L1 carrier frequency). The ranging code also serves as an additional measurement, and therefore increases availability and continuity of position fixes. Applying the correction data for satellite related errors (e.g., orbit, clock) or correction data concerning environmental con-

ditions (e.g., ionospheric delays) the accuracy of position solutions is increased and safety is improved by the integrity information, for example, by providing timely warnings if the system is not working correctly (Hofmann-Wellenhof et al. 2008).

2.4.1 Signal and Data Messages

The transmitted SBAS information has a 250 bits per second baseline data rate and is modulated onto the GPS-like ranging code. There are 61 different SBAS message types and currently not all of them are specified. These messages contain information on correction data like fast and long-term or ionospheric delay, ephemerides and almanac data. SBAS satellites transmit "use/do no use" information as well as correction data including user differential range estimate (UDRE) – an estimation of errors associated with satellites. Different message types will be updated within a defined interval (Hofmann-Wellenhof et al. 2008). To calculate protection levels (see Chapter 4) some of these message types are needed – their maximum update interval can be seen in Table 2.2, which are taken from RTCA (1999).

Table 2.2: SBAS message broadcast intervals

Message Type	**Data**	**Max. Update Interval** [s]
1	PRN mask	120
2 – 6, 24	UDRE indicator	6
2 – 5, 24	Fast corrections	60
24, 25	Long-term corrections	120
7	Fast correction degradation	120
10	Degradation parameters	120
18	Ionospheric grid mask	300
26	Ionospheric corrections	300

Each message's data block is split into an 8-bit preamble, a 6-bit message type identifier, 212-bit data field and a 24-bit parity field, which is illustrated in Figure 2.4. Depending

on the message type the data field contains different information (RTCA 1999). The transmitted bits are encoded by inserting redundant information. An output symbol stream twice the length of the input data bits is generated based on binary logic. This is called forward error correction (FEC). Therefore, the decoder is enabled to detect and correct errors of corrupted bits. Using a Viterbi decoder the most likely sequence of the message bits is found (Berglez 2013).

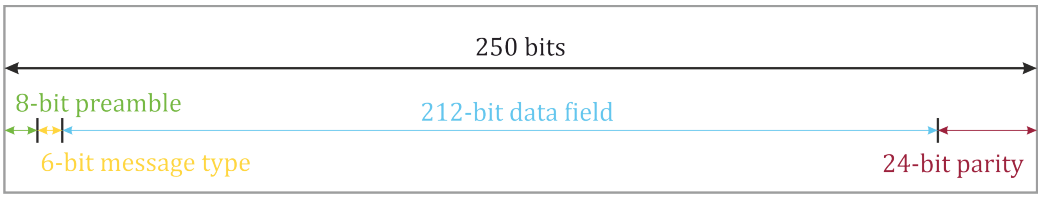

Figure 2.4: SBAS message data block format

The sent messages include the most recent information. However, to guarantee integrity if some messages are not received, degradation factors can be applied. For the calculation of protection levels the most important messages are:

Type 1: PRN Mask Assignments This message type holds information on which satellites are observed and for which corrections are included in the corresponding messages.

Type 2 – 5, 24: Fast Corrections Each message holds information about the fast corrections (e.g. clock correction) and the UDRE indicator (integrity information) for 13 observed satellites, so the number of messages sent depends on the number of observed satellites transmitted in message type 1. Long term corrections (e.g., orbit correction) can either be broadcasted in message type 24 or message type 25.

Type 7: Fast Correction Degradation Factor For each satellite mentioned in message type 1 the UDRE degradation factor is transmitted as well as the system latency.

Type 10: Degradation Factors Message This message type broadcasts other degradation factors (e.g., for range rate or ionospheric corrections).

Type 18: Ionospheric Grid Point Mask In this message's data field ionospheric grid points (IGPs) for which corrections are calculated are broadcasted.

Type 26: Ionospheric Delay Corrections Vertical delay estimates for the observed IGPs are transmitted in this message to calculate ionospheric delay corrections.

2.4.2 EGNOS

Since SBAS do not have a global coverage, there are multiple wide-area systems. The regional system in Europe is called European geostationary navigation overlay service (EGNOS). It is part of the European GNSS program developed by the European Union – fully delegated by the European Commission. In 1994 the program was approved by the European Council. It has been fully operational since 2009. EGNOS was designed to be concurrent with the other augmentation systems WAAS (America), MSAS (Japan) and GAGAN (India) (Ventura-Traveset et al. 2015).
The ground network consists of 40 ranging and integrity monitoring stations, which gather data from three geostationary satellites, as well as six navigation land earth stations and two mission control centers (GSA 2017a).
Like Galileo, EGNOS provides three services:

- Open Service: For applications like personal navigation (since October 2009)
- Safety-of-Life Service: Designed for applications when human lives depend on accuracy and integrity – primarily in aviation (since March 2011)

- Commercial Data Distribution Service: Via the EGNOS Data Access Service (EDAS) raw data and all EGNOS message corrections and integrity information in real-time are available (since July 2012)

EGNOS improves the performance of GPS by providing correction data and integrity information, especially for safety-of-life applications like in maritime or aviation as well as for precision farming. It meets the ICAO standards and is approved to be used in aviation for en-route navigation and during precision approaches because it particularly enhances the vertical precision. In the future EGNOS will be adapted to support Galileo and its service coverage area will be extended (ESA 2009).

3 Airspace and Flight Path

In aviation, airspaces are defined for the safety and control of aircrafts. The airspace above a federal territory is divided into multiple sectors, which are defined geographically and in height. Some of these are controlled airspaces in which an aircraft first needs clearance from the air traffic controller, and some of these are restricted airspaces which allow flights only in accordance with specific conditions, for example, military or emergency flights only. The geographical extensions of controlled airspaces and the limitations of restricted airspaces for Austria can be found in AIP Austria (2017). In Austria, UAVs with a guaranteed line of sight to the pilot are legally allowed in the uncontrolled airspace below 150 m altitude (see Section 1.5).

For DEMONA, the UAV is supposed to maneuver only within a predefined airspace along a certain trajectory. The airspace is therefore determined by the accuracy of the position of the aircraft and an extra safety margin on either side. The theoretical flight path is designed using waypoints from which turn points are derived considering the performance of the UAV.

The waypoint coordinates are given in WGS-84, which is the reference frame used for GPS and also the standard used in aviation (AIP Austria 2017). WGS-84 is an ellipsoidal coordinate system. A point can also be expressed by using Cartesian coordinates (see Section 3.1.1). Both systems describe the position of a point differently; Cartesian coordinates do not separate height or position, whereas ellipsoidal coordinates separate height and position by defining the height of a point along the plumb line from the reference

ellipsoid to the surface. Therefore, the calculation of the path lengths differs depending on the coordinate system used. Since the UAV is supposed to maneuver within a certain height range, the differences in the results between the computations are verified.
To determine if a UAV is located within its protected airspace, the deviation in across track and in height between the UAV position and the predefined flight path is needed.

3.1 Coordinate Systems

In general, there is a difference between coordinate systems and coordinate frames. The first describes the theoretical definition, the latter the realization of that system. An example of a coordinate system is the International Terrestrial Reference System (ITRS) – its regularly updated realization is the International Terrestrial Reference Frame (ITRF) (Hofmann-Wellenhof and Moritz 2006).
A coordinate system is defined by an origin and the orientation of at least two axes so that a consistent representation of a given point in the system is guaranteed. It can either be terrestrial or celestial, however, the terrestrial system is better suited for applications concerning any flights with a UAV because a UAV moves within the vicinity of the earth's surface.
The so-called earth-centered, earth-fixed (ECEF) coordinate system is a global system with the origin at the earth's geocenter. Its Z-axis is defined to be coincident with the mean direction of the earth's rotation axis. The X-axis corresponds to the intersection line between the equatorial plane and the Greenwich meridian. Therefore, the Y-axis is orthogonal to the X- and Z-axis to complete a right-handed system (Hofmann-Wellenhof et al. 2003).
The WGS-84 is a geocentric ellipsoid of revolution. It coincides with the ITRF2014 (which is the latest edition) within a few centimeters and is defined by using the current four parameters in Table 3.1, which were taken from Hofmann-Wellenhof et al. (2008).

Table 3.1: Parameters of the WGS-84 ellipsoid

Parameter		Value	Description
a	=	6 378 137.0 m	Semimajor axis of the ellipsoid
f	=	1 / 298.257 223 563	Flattening of the ellipsoid
ω_e	=	$7\,292\,115 \cdot 10^{-11}$ rad s^{-1}	Angular velocity of the earth
GM	=	$3\,986\,004.418 \cdot 10^{8}$ m^3 s^{-2}	Earth's gravitational constant

3.1.1 Ellipsoidal and Cartesian Coordinates

As shown in Figure 3.1 a point can either be defined using Cartesian coordinates (X, Y, Z) or coordinates which are related to an ellipsoid (φ, λ, h). In order to describe positions on the reference ellipsoid, definitions of parallels and meridians are required; often the meridian of Greenwich and the equator are used.

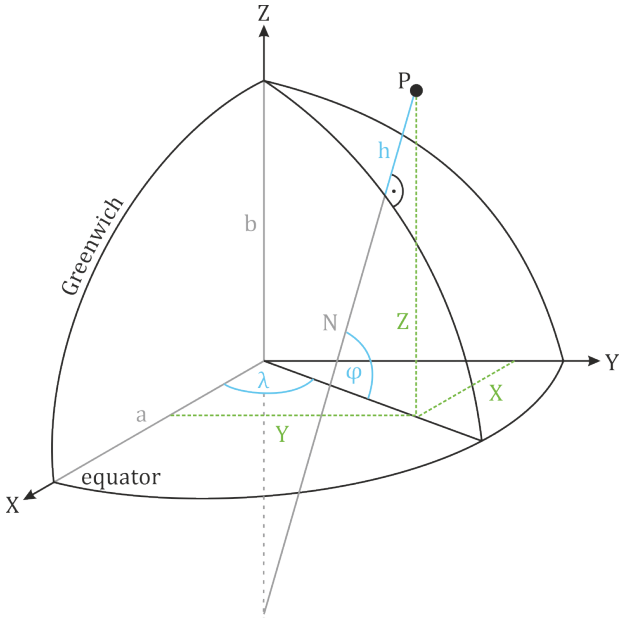

Figure 3.1: Cartesian and ellipsoidal terrestrial coordinate system

However, transformations between the systems are possible (Hofmann-Wellenhof and Moritz 2006). Using the semiaxes of the ellipsoid a and b and the radius of curvature

$$N = \frac{a^2}{\sqrt{a^2 \cdot \cos^2 \varphi + b^2 \cdot \sin^2 \varphi}} \,, \tag{3.1}$$

the Cartesian coordinates can be calculated directly from the ellipsoidal system with

$$\begin{pmatrix} X \\ Y \\ Z \end{pmatrix} = \begin{bmatrix} (N+h) \cdot \cos\varphi \cdot \cos\lambda \\ (N+h) \cdot \cos\varphi \cdot \sin\lambda \\ \left(\frac{b^2}{a^2} \cdot N + h\right) \cdot \sin\varphi \end{bmatrix} \quad . \tag{3.2}$$

The computation of the transformation from Cartesian to ellipsoidal coordinates usually requires an iteration to determine the latitude and height, whereas the longitude can be derived directly. The ellipsoidal coordinates are obtained by

$$\begin{aligned} \varphi &= \arctan \frac{Z}{\sqrt{X^2+Y^2}} \cdot \left(1 - e^2 \cdot \frac{N}{N+h}\right)^{-1} \quad , \\ \lambda &= \arctan \frac{Y}{X} \quad , \\ h &= \frac{\sqrt{X^2+Y^2}}{\cos\varphi} - N \quad , \end{aligned} \tag{3.3}$$

where the first numerical eccentricity e is described by

$$e^2 = \frac{a^2 - b^2}{a^2} \quad . \tag{3.4}$$

A closed equation also exists for the transformation of the latitude φ (Hofmann-Wellenhof and Moritz 2006).

3.1.2 Local-Level Frame

A local-level frame is defined anywhere on the surface as a direct reference to a geodetic observation, this means the origin is arbitrary. The axes directions are north (**n**), east (**e**) and up (**u**) or down (**d**), depending if a right or left-handed coordinate system is required.

The only difference is the sign:

$$\mathbf{u} = \begin{pmatrix} \cos\varphi \cdot \cos\lambda \\ \cos\varphi \cdot \sin\lambda \\ \sin\varphi \end{pmatrix} \quad \text{or} \quad \mathbf{d} = \begin{pmatrix} -\cos\varphi \cdot \cos\lambda \\ -\cos\varphi \cdot \sin\lambda \\ -\sin\varphi \end{pmatrix} . \tag{3.5}$$

Using Eq. (3.5) the other two axes can be derived by using the partial derivatives

$$\begin{aligned} \mathbf{n} &= \frac{-\partial \mathbf{d}}{\partial \varphi} , \\ \mathbf{e} &= \frac{-1}{\cos\varphi} \cdot \frac{\partial \mathbf{d}}{\partial \lambda} . \end{aligned} \tag{3.6}$$

In Figure 3.2 the local-level frame is shown in reference to the ECEF coordinate system.

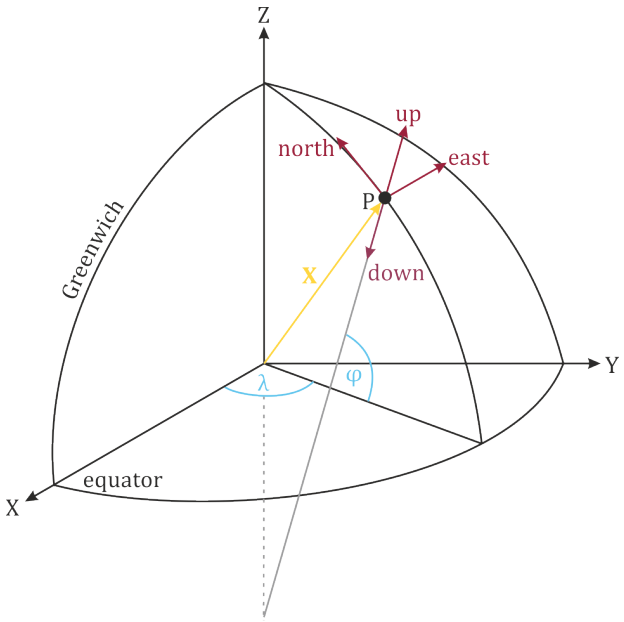

Figure 3.2: Local-level frame and terrestrial global coordinate system

Since the origin is arbitrary, only a difference vector may be transformed from the local-level frame to the terrestrial equatorial system, by multiplying it with the rotation matrix $\mathbf{R}$,

where the sign of the last column depends if **d** (in this case) or **u** is used and yields

$$\mathbf{R} = \begin{bmatrix} -\sin\varphi \cdot \cos\lambda & -\sin\lambda & -\cos\varphi \cdot \cos\lambda \\ -\sin\varphi \cdot \sin\lambda & \cos\lambda & -\cos\varphi \cdot \sin\lambda \\ \cos\varphi & 0 & -\sin\varphi \end{bmatrix}, \tag{3.7}$$

where φ and λ are the (global) ellipsoidal coordinates of the origin of the local-level system.

3.2 Spatial Distances

Geodesy is the science behind the measurement and representation of the earth. By measuring angles and distances, coordinates can be calculated by using the so-called direct problem of geodesy. The indirect problem deals with the calculation of angles and distances between a given arrival and departure point. These can be calculated either for Cartesian or for ellipsoidal coordinate systems. The indirect problem is an iterative solution if ellipsoidal coordinates are determined (RTCA 1999). These equations find the shortest path along the surface of the ellipsoid between two given points, i.e., a geodesic. A geodesic defines a plane which contains the center of the sphere. In the case of an ellipsoid of revolution, i.e., it is rotating around its minor axis, these can only be the meridians and the equator.

The position and height are separated for calculations on the ellipsoid. A UAV is flying in a certain altitude above ground, which means for the actual height h the distance flown has to be reduced to the ellipsoid, as shown in Figure 3.3). According to Hofmann-Wellenhof and Moritz (2006), the spatial distance S_R, calculated with the equations for solving the indirect problem using Cartesian coordinates, is reduced to the chord distance S_0 using

$\Delta h = h_A - h_B$ and which is calculated by

$$S_0 = \sqrt{\frac{S_R^2 - \Delta h^2}{\left(1 + \frac{h_A}{R}\right) \cdot \left(1 + \frac{h_B}{R}\right)}} \ . \tag{3.8}$$

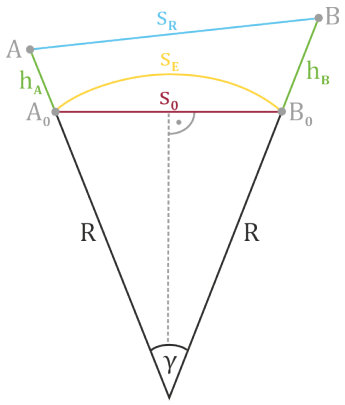

Figure 3.3: Reduction of spatial distances

R is the radius of the curvature at any azimuth α_{AB} and can be derived from Euler's equation (Torge and Müller 2012). It can be written as

$$R = \frac{N}{1 + e'^2 \cdot \cos^2 \lambda_A \cdot \cos^2 \alpha_{AB}} \ , \tag{3.9}$$

where N corresponds to Eq. (3.1) and the second numerical eccentricity e' is computed by

$$e'^2 = \frac{a2 - b^2}{b^2} \ . \tag{3.10}$$

$S_E = R \cdot \gamma$ corresponds to the geodesic calculated using the equations for the ellipsoidal indirect problem (RTCA 1999). γ is the central angle of the arc S_E and is derived by

$$\gamma = 2 \cdot \arcsin \frac{S_0}{2 \cdot R} \ . \tag{3.11}$$

Cartesian coordinates do not separate position and height as ellipsoidal systems do, i.e., coordinates can be considered as a vector which is able to describe the motion of an object in 3D. A UAV is a flying object, which means the height is a factor that must be considered. Therefore, investigations were performed to evaluate the difference in path lengths by using either ellipsoidal or Cartesian coordinates.

The differences were calculated for different lengths and azimuths on the surface of the sphere. In Figure 3.4, the results for the differences in ellipsoidal and Cartesian path lengths are shown. For distances up to 1 km the deviations are less than 1 cm.

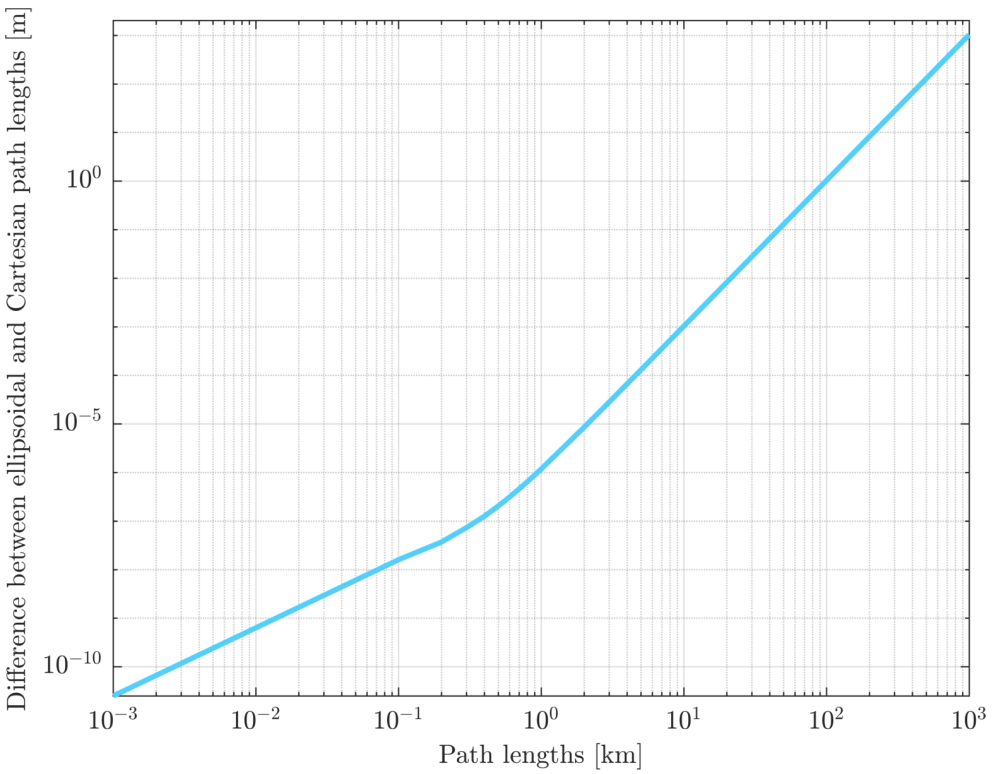

Figure 3.4: Differences between ellipsoidal and Cartesian path lengths

The same behavior is notable in the results for different azimuths in Figure 3.5, which are calculated with reference to azimuth = 0°, as well as when the spatial distances are reduced to the surface of the ellipsoid, as shown in Figure 3.6.

For the different heights, there is almost no distinction in the differences up to a distance

of around 200 km. For Cartesian path lengths, the difference was calculated between the chord distances, for ellipsoidal paths between the geodesic distance.

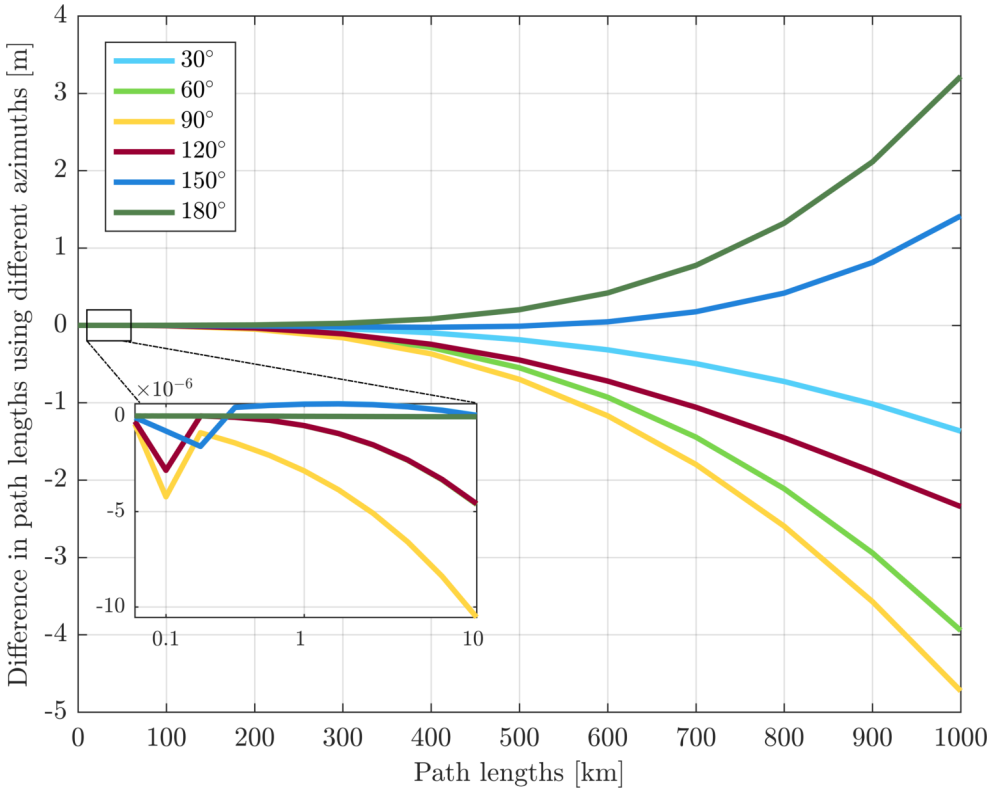

Figure 3.5: Differences of path lengths with different azimuths

In this thesis, the UAV is supposed to fly a maximum distance between 10 km and 15 km in total at an altitude of up to 150 m above the ground. At that distance neither Cartesian nor ellipsoidal path length differences between heights of 100 m and 1000 m are bigger than 10^{-5} m. The distinction between the distances, which were calculated using different methods, is 1 mm at 10 km and 8 mm at 20 km. These values are negligible compared to the achievable accuracy (see Section 6.2.2) and the calculated protection levels (Chapter 4). Therefore, the reduction of the spatial distances onto the ellipsoid can be neglected. For further computations the Cartesian formulas are used.

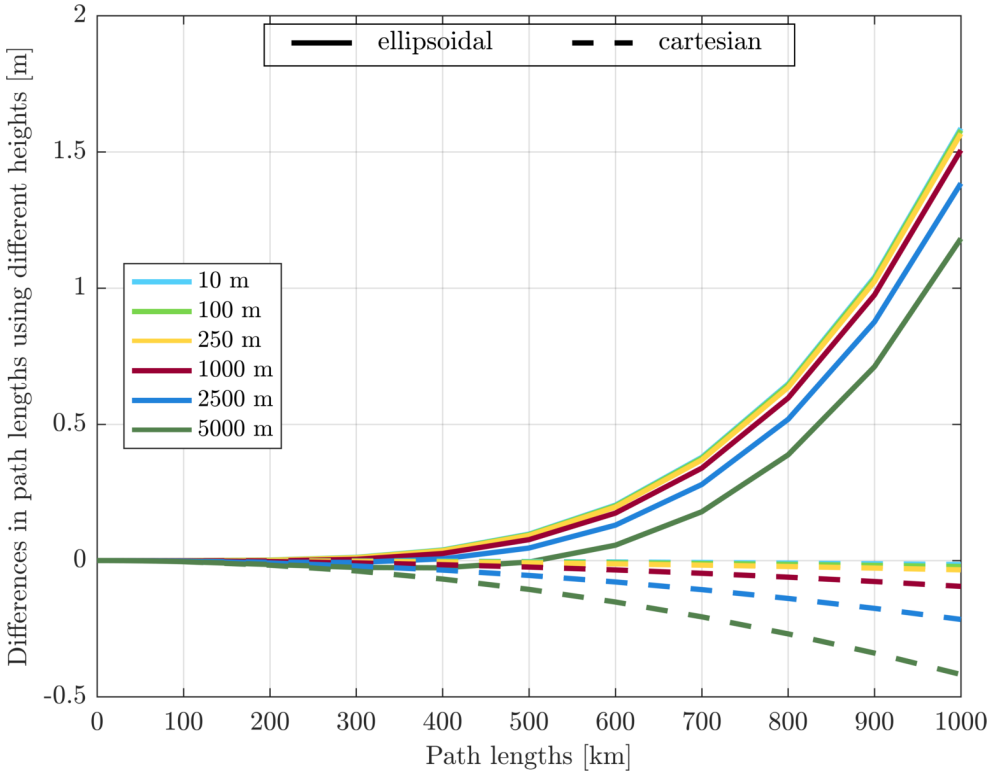

Figure 3.6: Differences of path lengths for different heights

3.3 Trajectory

A reference trajectory is needed to determine the deviation of the UAV from its defined flight path. This trajectory is computed using waypoints along the defined flight path. These waypoints either divide long stretches of straight paths or define a change in the flight path, i.e., turns. In aviation, waypoints are defined by path terminators (ICAO 2006). There are in total twelve different path terminator types, each representing which procedure an area navigation (RNAV) approved aircraft is supposed to fly to define a specific ground track, including:

- Course from a fix to an altitude (FA) Route segment that starts at a waypoint and terminates at an altitude at an unspecified position (shown in Figure 3.7)

- Direct to a fix (DF) Non-predictable flight path direct from an unspecified position to a specified waypoint
- Course to an altitude (CA) Course for a route segment that terminates at an unspecified position when a specified altitude is reached
- Constant radius arc to a fix (RF) Circular path with a defined start and end waypoint and a constant radius around an arc center

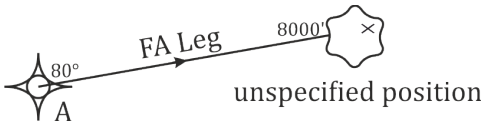

Figure 3.7: Path terminator: course from a fix to an altitude (RF)

Planning a reference trajectory (and because during flight, the positions are supposed to be constantly known due to the usage of GNSS), not all path terminators (i.e., none of those that start or end at an undefined position and/or altitude) are suitable or useful for UAVs (in case of DEMONA). This leaves only two which can be used:

- Initial fix (IF) Start of the procedure but does not define a track itself
- Track to a fix (TF) Straight route segment (geodesic path) between two waypoints with given coordinates (shown in Figure 3.8)

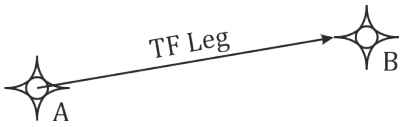

Figure 3.8: Path terminator: track to a fix (TF)

The waypoints are also defined as fly-by or fly-over points. Fly-by waypoints are not supposed to be flown over, consequently the turn has to be initiated before. Therefore,

turn points must be determined. In RTCA (1999) fly-by turns are defined as turns with heading changes less than or equal to 120° (for turns greater than that are no specific requirements defined).

In aviation, waypoints are defined on aeronautical charts with their coordinates in WGS-84 and additional information including altitude, turn direction or speed. In the case of a UAV, some of that information (for example, waypoint identifier or navigation specification) is not necessary and does not need to be included. However, information defining a waypoint as a fly-over or a fly-by is necessary.

For a fly-by turn, the earliest and latest turn points before and after the supposed waypoint are computed. The mean value of those points is used to calculate a turn initiation distance for the reference trajectory given as

$$Y\ [nm] = R_{turn} \cdot \tan\frac{\alpha}{2} \tag{3.12}$$

with the turn radius

$$R_{turn}\ [nm] = (1.458 \cdot 10^{-5}) \cdot \frac{v_{ground}^2}{\tan\varphi}\ . \tag{3.13}$$

Since Eq. (3.12) requires the true ground speed v_{ground} [kn] and bank angle φ [°] (nominal: 15°) the actual flight path is computed in real-time during flight. The track change α results from the difference of the current and the next course. If the actual flight path deviates from a waypoint, there is a transition area – as shown in Figure 3.9 – which is the region outlined by the arc with the radius R_{turn} and the initiation distance Y between the turn point and the waypoint. Y can be defined in either direction of the waypoint along the trajectory. This region is added to the threshold of the protected airspace when a turn is performed.

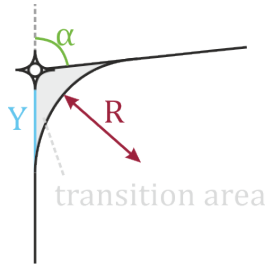

Figure 3.9: Theoretical transition area for a fly-by waypoint

3.4 Protected Airspace

The UAV is supposed to follow the defined reference trajectory but in reality, it will slightly deviate from the planned flight path, which can be a result of, for example, gusts of wind, the accuracy of the position tracking and manual piloting. Accordingly, an airspace has to be defined. Within this protected area the UAV is permitted to maneuver within a certain threshold of the reference trajectory without being considered off-track. This margin was set to a maximum of 250 m across track and 100 m in height. This is a result of considering the possible accuracy, the calculated protection levels and a certain buffer.

To determine if the UAV is located within the protected airspace, its position is calculated with reference to the planned trajectory. These calculations are performed using vector projections and calculations. A benefit of this method is that it avoids too many transformations between different coordinate systems (see Section 3.1).

An intersection is calculated between the actual position and the normal level to the reference trajectory in this point. Figure 3.10 shows the vector system in theory. The difference vector between the UAV position and the intersection point at the trajectory is split into its horizontal (across track) and vertical (height) components after being transformed into a local-level system (see Section 3.1.2). The origin of the local-level system is at the UAV's current position.

The protected airspace is defined as an ellipse around the intersection point where the semiaxes represent the tolerated deviation in height and across track (more in Section 5.4).

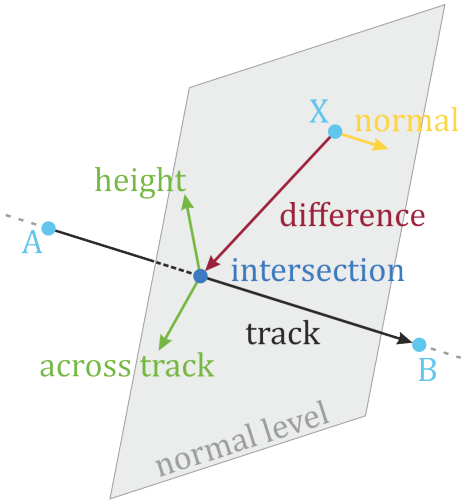

Figure 3.10: Intersection between a straight line and a point (vector system)

The position of the UAV is within the ellipse, and therefore within the protected airspace, if the length of the difference vector does not exceed the radius at the particular angle of the UAV position, as shown in Figure 3.11.

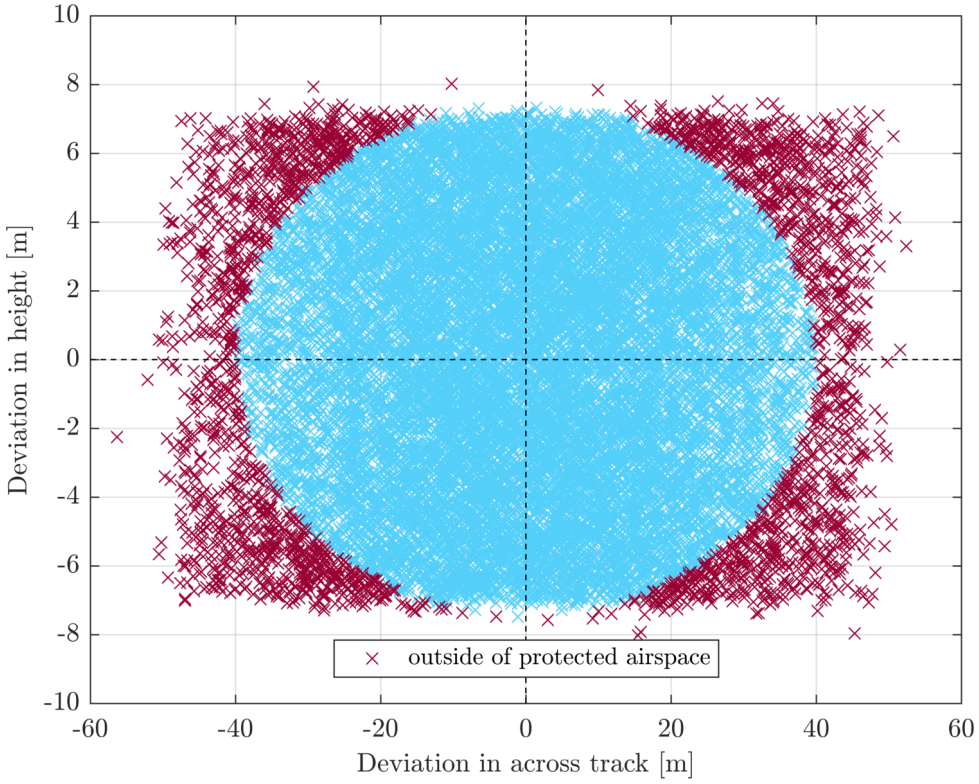

Figure 3.11: Deviations from the planned flight path in across track and height

4 Protection Levels and Safety Envelope

The measure of trust in the correctness of the provided information is called integrity. This is the ability to issue timely warnings when the system should not be used. The integrity concept can be expressed by integrity parameters, such as the alert limit, time to alert, integrity risk and protection levels. The alert limit expresses the maximum error tolerance, time to alert is the maximum elapsed time until the warning is issued and the integrity risk shows the probability that the alert limit is exceeded. A protection level is the statistical bound error that describes the integrity (risk) mathematically (Hofmann-Wellenhof et al. 2008). Integrity is especially important for safety critical applications, such as precision approach and landing in aviation or harbor maneuvering in maritime. During those applications integrity, accuracy, continuity and availability of a position fix are critical.

SBAS, such as EGNOS, as described in Section 2.4, provides integrity information and correction data for GPS. The latter consists of fast corrections, which are rapidly changing errors, for example, GPS clock errors, and of long-term corrections, which are slowly varying like ephemeris errors or the ionospheric delay model. Protection levels, which are explained further in Section 4.1, can be calculated according to RTCA (1999), Appendix J based on SBAS correction data.

In addition, a safety envelope can be calculated to account for the aircraft's dimensions

(i.e., nose, tail and wing tips) depending on its attitude instead of only considering the position of the antenna. Compared to the magnitude of the protection levels the extension of the safety envelope is low. However, both protection levels and safety envelope are added to the deviations of the UAV from the reference flight path. The probability that the true position of an object lies within the protection level is $1 - 10^{-7}$ (RTCA 1999). This means that if they are included in the horizontal and vertical deviations, the probability that the true deviation lies within is at least 99.9 %.

4.1 Protection Levels

A protection level is a measure for the bounds of the position error. It is a predictable value because it is not affected by actual measurements but it is a function of the satellite and user geometry and the expected error characteristics (RTCA 1999). They show the maximum possible error at the receiver with a probability of $1 - 10^{-7}$. Protection levels are divided into vertical and horizontal protection levels. The horizontal protection level is defined as the radius of a circle in the horizontal plane with its center at the true position. The vertical protection level equals half the length of a segment on the vertical axis which is perpendicular to the horizontal plane, as shown in Figure 4.1.

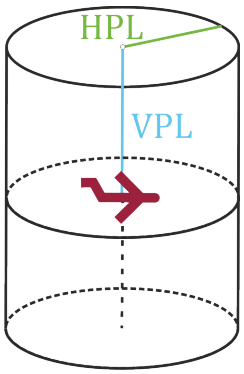

Figure 4.1: Schematic representation of the horizontal and vertical protection level

The calculation of protection levels according to RTCA (1999) is based on a least squares

adjustment to determine position errors using pseudorange errors. The connection between measurements and the user position is given by

$$\mathbf{z} = \mathbf{G} \cdot \mathbf{x} + \mathbf{v} \ , \tag{4.1}$$

where $\mathbf{z}$ equals the measurement vector (containing pseudorange measurements) and $\mathbf{v}$ accounts for the measurement errors. The vector $\mathbf{x}$ holds the position in local coordinates (north, east, up) and the combined clock bias. The observation matrix $\mathbf{G}$ consists of the observation equations for the line-of-sight vectors between the user and each satellite. For the i$^{\text{th}}$ satellite the i$^{\text{th}}$ row can be written in terms of the elevation E and the azimuth Az between the i$^{\text{th}}$ satellite and the receiver as

$$\mathbf{G}_i = \begin{bmatrix} -\cos E_i \cdot \sin Az_i & -\cos E_i \cdot \cos Az_i & -\sin E_i & 1 \end{bmatrix} \ , \tag{4.2}$$

where the last column accounts for the clock bias. The position solution is therefore estimated using a least squares adjustment in terms of best linear unbiased estimate (BLUE) with

$$\hat{\mathbf{x}} = (\mathbf{G}^T \cdot \mathbf{W} \cdot \mathbf{G})^{-1} \cdot \mathbf{G}^T \cdot \mathbf{W} \cdot \mathbf{z} = \mathbf{S} \cdot \mathbf{z} \ . \tag{4.3}$$

The weight matrix $\mathbf{W}$ is the inverse measurement covariance matrix (Walter et al. 1997). The measurements are assumed to be uncorrelated, and therefore the weight matrix can be written as

$$\mathbf{W}^{-1} = \begin{bmatrix} \sigma_i^2 & 0 & \dots & 0 \\ 0 & \sigma_i^2 & \dots & 0 \\ \vdots & \ddots & \ddots & \vdots \\ 0 & \dots & 0 & \sigma_i^2 \end{bmatrix} \tag{4.4}$$

with σ_i^2 being the variance of the pseudorange error σ_i (Walter et al. 1997). The matrix $\mathbf{S}$ represents the relation between the measurement errors and the position errors and reads

$$\mathbf{S} = \begin{bmatrix} s_{east,1} & s_{east,2} & \dots & s_{east,N} \\ s_{north,1} & s_{north,2} & \dots & s_{north,N} \\ s_{up,1} & s_{up,2} & \dots & s_{up,N} \\ s_{t,1} & s_{t,2} & \dots & s_{t,N} \end{bmatrix} . \tag{4.5}$$

The elements of the matrix $\mathbf{S}$ are used to calculate the variances of model distribution that overbounds the true distribution in the east d_{east}^2, north d_{north}^2 and vertical d_{up}^2 axis as well as the variance of the model distribution in the east and north axis $d_{east,north}$ (RTCA 1999), which yields

$$d_{east}^2 = \sum_{i=1}^{N} s_{east,i}^2 \cdot \sigma_i^2 \ , \tag{4.6}$$

$$d_{north}^2 = \sum_{i=1}^{N} s_{north,i}^2 \cdot \sigma_i^2 \ , \tag{4.7}$$

$$d_{up}^2 = \sum_{i=1}^{N} s_{up,i}^2 \cdot \sigma_i^2 \ , \tag{4.8}$$

$$d_{east,north} = \sum_{i=1}^{N} s_{east} \cdot s_{north} \cdot \sigma_i^2 \ . \tag{4.9}$$

The horizontal protection level *HPL* and vertical protection level *VPL* are then calculated using

$$HPL = K_H \cdot d_{major} \ , \tag{4.10}$$

$$VPL = K_V \cdot d_{up} \tag{4.11}$$

with

$$d_{major} = \frac{d_{east}^2 + d_{north}^2}{2} + \sqrt{\left(\frac{d_{east}^2 - d_{north}^2}{2}\right)^2 + d_{east,north}^2} \,. \tag{4.12}$$

K is a bound for the user position using a normal distribution in one dimension with a probability of 10^{-7} for the vertical and $2 \cdot 10^{-9}$ for the horizontal dimension. K_H equals 6 (for precision approach) and K_V is 5.33 (RTCA 1999). The value for K_H for the precision approach was used instead of $K_H = 6.18$ for en-route navigation so the calculated values for the protection levels are smaller. Usually the protection levels lie within a magnitude of 5 m to 30 m. During the course of DEMONA these values for K might need to be adapted after some test flights with a UAV because the used values are defined for flights with manned aircraft.

4.1.1 SBAS-based Protection Levels

The variance of pseudorange error σ_i^2 is calculated based on RTCA (1999) using data from SBAS messages (see Section 2.4.1). It is assembled by the variance of the fast and long-term corrections $\sigma_{i,flt}^2$, the variances of the ionospheric delay $\sigma_{i,UIRE}^2$ and tropospheric delay $\sigma_{i_tropo}^2$ and the variance of the airborne receiver error $\sigma_{i,air}^2$ and is calculated with

$$\sigma_i^2 = \sigma_{i,flt}^2 + \sigma_{i,UIRE}^2 + \sigma_{i,air}^2 + \sigma_{i,tropo}^2 \,, \tag{4.13}$$

for each satellite i.

Variance of the fast and long-term corrections σ_{flt}^2

The variance of the fast corrections σ_{UDRE}^2 is transmitted via messages type 2 to 5 (fast corrections message). In principle, the most recent information is broadcasted. However, if a message is missed, the degradation of the data is modeled, using, for example, the

degradation factor from message type 7 (fast correction degradation factor message), so the integrity can be ensured in any case. Depending on the root sum square (RSS) flag for the user differential range estimate (UDRE) RSS_{UDRE}, which is transmitted via message type 10 (degradation factors message), $\sigma^2_{i,FLT}$ is calculated using degradation data for fast corrections ε_{fc}, for range rate corrections ε_{rrc}, for the long-term corrections ε_{ltc} and in case the fast or long-term correction have timed out for precision approach also for en-route through non-precision approach applications ε_{er}:

$$\sigma^2_{flt} = \begin{cases} (\sigma_{UDRE} \cdot \delta_{UDRE} + \varepsilon_{fc} + \varepsilon_{rrc} + \varepsilon_{ltc} + \varepsilon_{er})^2 & \text{for } RSS_{UDRE} = 0 \\ (\sigma_{UDRE} \cdot \delta_{UDRE})^2 + \varepsilon^2_{fc} + \varepsilon^2_{rrc} + \varepsilon^2_{ltc} + \varepsilon^2_{er} & \text{for } RSS_{UDRE} = 1 \end{cases} , \tag{4.14}$$

where δ_{UDRE} is a factor to increase σ_{UDRE} in certain areas and is transmitted in message type 27 (WAAS service message).

Variance of the ionospheric delay σ^2_{UIRE}

Message type 18 (ionospheric grid point masks message) transmits the ionospheric grid points for which the variances of the grid ionospheric vertical error (GIVE) σ^2_{GIVE} is broadcasted via message type 26 (ionospheric delay corrections message). Using this data the coordinates of the ionospheric pierce point (IPP) can be calculated according to RTCA (1999) using the elevation E and azimuth Az with

$$\varphi_{PP} = -\arcsin\left(\sin\varphi_{User} \cdot \cos\psi_{PP} + \cos\varphi_{User} \cdot \sin\psi_{PP} \cdot \cos Az\right) , \tag{4.15}$$

$$\lambda_{PP} = \lambda_{User} + \arcsin\left(\frac{\sin\psi_{PP} \cdot \sin Az}{\cos\varphi_{PP}}\right) . \tag{4.16}$$

The IPP equals the coordinates of the point where the signal path between the transmitting satellite and the user position (φ_{User}, λ_{User}) intersects with a (modeled) thin shell of the ionosphere in a height h_I, where all the electrons are assumed to be concentrated, i.e., the height of the maximum electron density (according to RTCA (1999) $h_I = 350$ km). ψ_{PP}

equals the angle between the user position and the projection of the IPP onto the earth and reads

$$\psi_{PP} = \frac{\pi}{2} - E - \arcsin\left(\frac{R}{R+h_I} \cdot \cos E\right) , \tag{4.17}$$

where R is the radius of the earth. A model of this geometry is shown in Figure 4.2.

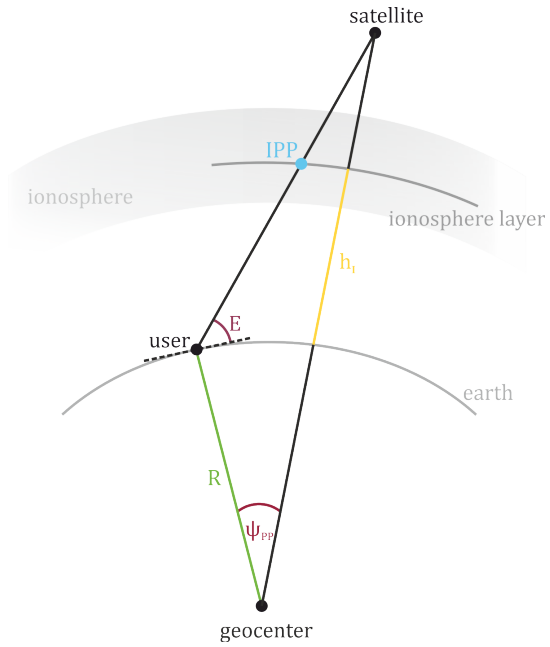

Figure 4.2: Geometry of the ionospheric pierce point

Depending on the coordinates of the IPP, grid points are selected from the IGP mask in message type 18. Their calculated model variance of the ionospheric vertical delays $\sigma^2_{ionogrid}$ is used to interpolate the variance of the user ionospheric vertical delay σ^2_{UIVE} at the user position. More details can be found in RTCA (1999). Together with the obliquity factor

$$F_{pp} = \left(1 - \left(\frac{R \cdot \cos E}{R+h_I}\right)^2\right)^{-\frac{1}{2}} , \tag{4.18}$$

the variance of the ionospheric delay σ^2_{UIRE} can be calculated by

$$\sigma^2_{UIRE} = F^2_{pp} \cdot \sigma^2_{UIVE} \ . \tag{4.19}$$

The variance of the ionospheric delay is the only frequency dependent variable. If the position solution is derived for any frequency other than GPS L1 the σ^2_{UIRE} should be scaled (Shau-Shiun 2002), like for L5 by

$$\sigma_{UIRE,L5} = \left(\frac{f_1}{f_5}\right)^2 \cdot \sigma_{UIVE,L1} \ . \tag{4.20}$$

In this thesis, multi-frequency observations were not considered. In the future, however, the algorithm should be expanded towards multi-frequencies. In DEMONA, GPS L1 observations are used as well as Galileo E1 observations. Since currently Galileo signals are not considered for the SBAS-based protection levels, the calculation was only based on GPS measurements.

Variance of the tropospheric delay σ^2_{tropo}

Because the tropospheric refraction is a local phenomenon (it is depending on temperature, air pressure and humidity), it needs to be calculated by the user solely based on the elevation angle E (for elevations greater than 5°) between the user and the satellite i. Therefore, the variance of the tropospheric delay corresponds to

$$\sigma^2_{tropo} = (\sigma_{TVE} \cdot m(E_i))^2 \tag{4.21}$$

with the tropospheric vertical error $\sigma_{TVE} = 0.12$ m (RTCA 1999). Black and Eisner's mapping function

$$m(E_i) = \frac{1.001}{\sqrt{0.002001 + \sin^2 E_i}} \tag{4.22}$$

is used to calculate the slant delay error (Conley et al. 2006).

Variance of the airborne receiver error σ^2_{air}

Depending on the class of the GPS equipment, according to RTCA (1999), the variance of the airborne receiver error is either represented with a standard value of 25 m^2 or in case ionospheric corrections are applied by

$$\sigma^2_{air} = \sigma^2_{mp} + \sigma^2_{noise}(SNR) \ . \tag{4.23}$$

Here the latter is the case. Therefore, the variance of the multipath error

$$\sigma^2_{mp} = 0.2 \cdot \mathrm{e}^{-E_i/75} \tag{4.24}$$

as well as the GPS tracking accuracy of the receiver for the current signal-to-noise ratio $\sigma^2_{noise}(SNR)$ are needed (RTCA 1999). The tracking accuracy is calculated using

$$\sigma_{noise}(SNR) = \lambda_c \cdot \sqrt{\frac{B \cdot d}{2 \cdot {}^{C}/_{N0}} \cdot \left(1 + \frac{2}{(2-d) \cdot {}^{C}/_{N0} \cdot T_I}\right)} \ , \tag{4.25}$$

where B is the noise of the bandwidth in Hertz, T_I equals the coherent integration time in seconds and d defines the correlation spacing (Hofmann-Wellenhof et al. 2008). For scaling chips to meters the wavelength of the pseudorandom noise (PRN) code λ_c is used which equals 293.05 m for the C/A code. The signal-to-noise ratio (SNR) is the ratio of the received signal power to the noise power at the antenna (in decibel), whereas the carrier-to noise power density ratio (C/N0) is the ratio between the carrier power and the noise power after filtering (in decibel per Hertz).

4.1.2 Galileo-based Protection Levels

Currently SBAS is only transmitting information for GPS L1. It can take up to 300 seconds to receive all necessary SBAS messages to calculate protection levels. To compensate the time needed to receive all required SBAS data messages – which means no protection levels can be calculate – the option was considered to additionally use Galileo data. Galileo transmits its signal-in-space accuracy (SISA) with its navigation message. SISA is a prediction of satellite clock and ephemeris accuracy and equals the minimum standard deviation for the signal-in-space error. The transmitted SISA value can be encoded according to European Union (2016), which means as an index it follows a step function, i.e., it is only available for fixed values. However, it must be noted that the ESA has not made its final decision on the definition and usage of SISA. As of December 2017, a nominal value of 3.12 m is distributed with the navigation message.
Following Kneissel and Stöber (2010) SISA plus the variance of the remaining errors $\sigma^2_{u,L,i}$ correspond to the variance of the pseudorange error σ^2_i,

$$\sigma^2_i \hat{=} SISA^2 + \sigma^2_{u,L,i} \ . \tag{4.26}$$

The variance of the remaining errors includes, for example, the variances of the ionospheric and tropospheric delay errors or the variance of the airborne receiver error. Therefore, SISA can be compared with the variance of the fast and long-term corrections σ^2_{flt}. However, Eq. (4.26) is only true for the physical meaning but not numerically. A reason for that is, for example, the different satellite constellation (see Section 2.2 and Section 2.3). Since the SISA is defined as an index and no degradation factors are applied, it does not show the same accuracy as the variance for the fast and long-term corrections.
In simulations the Galileo-based protection levels have been calculated using SISA. The variance of the remaining errors $\sigma_{u,L,i}$ was derived using a standard value for the variance of the ionospheric delay depending on the elevation angle, and using a mean value for

the variance of the airborne receiver error. The variance of the tropospheric delay was calculated based on the elevation angle according to Eq. (4.21). Additionally azimuth and elevation to the satellite from the user position were used. Data sets for each Galileo satellite as well as information from SBAS were retrieved for the same time, day and position. In Figure 4.3 it can be seen, that depending on the SISA the protection levels follow the same course as the SBAS-based protection levels – each of those values were calculated for seven visible satellites for each Galileo and GPS. The difference in the actual size of the protection levels (especially for the horizontal protection level) is a result of the different elevation angles, and therefore a different geometry between user and visible satellites – as can be seen in the skyplots in Figure 4.4.

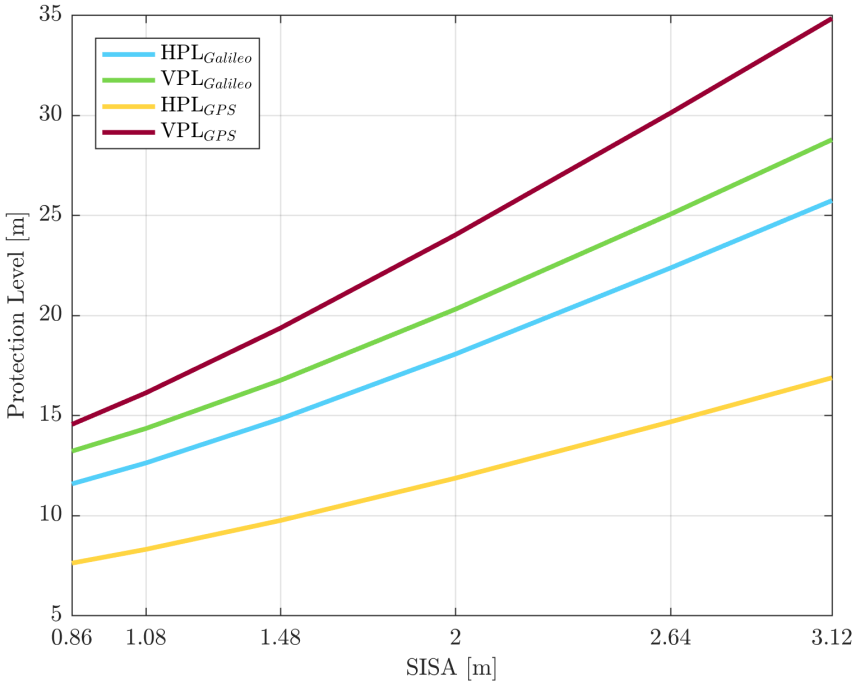

Figure 4.3: Simulation results for Galileo-based protection levels (for seven satellites)

Depending on the number of satellites used the value for the Galileo-based protection level changes. Simulations were calculated with four to seven satellites, where the best results were achieved with seven satellites. Because Galileo has not reached full operational capa-

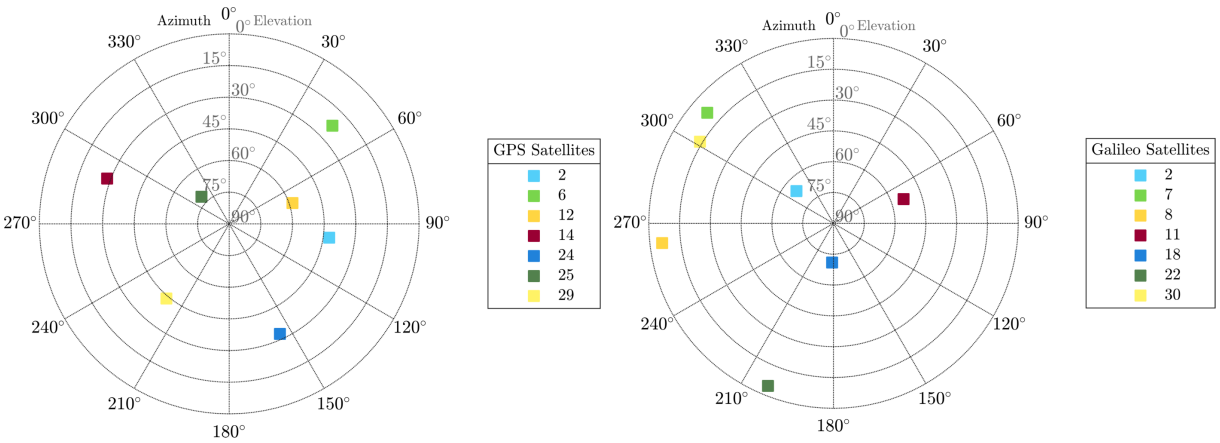

(a) GPS satellites

(b) Galileo satellites

Figure 4.4: Skyplots for visible GPS and Galileo satellites used in simulations

bility yet, only around four satellites can be observed simultaneously from one observation site. This means that even though acceptable results were achieved in simulations, the usage of Galileo-based protection levels is only recommended when at least four satellites are visible. However, more tracked satellites lead (normally) to a better geometry which then results in lower protection levels. This means if Galileo-based protection levels are used, the user must be aware that fewer tracked satellites lead to higher protection levels.

4.2 Safety Envelope

The position of the UAV is only determined for the antenna position. However, depending on the attitude of the UAV, parts of its dimensions also contribute to the deviations in across track and height. Consequently, a safety envelope is calculated to consider the UAV dimensions in the absolute deviations. Therefore, the UAV is assumed as a cuboid – as represented in Figure 4.5. If the antenna is not coinciding with the origin, the lever arm between antenna and origin of the body frame has to be considered.

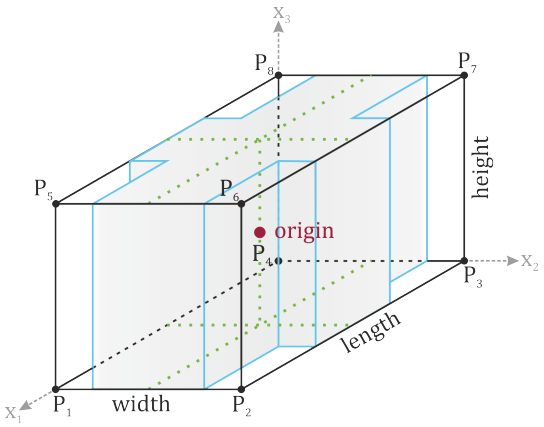

Figure 4.5: Graphical representation of the safety envelope

The body frame is a coordinate system that originates at a specific point within an object. Usually the right-handed coordinate axes coincide with the rotation axes of the object. In Figure 4.6 the coordinate axes and attitude parameters roll, pitch and yaw of the body frame are shown graphically for a fixed-wing aircraft. In the body frame of the UAV the

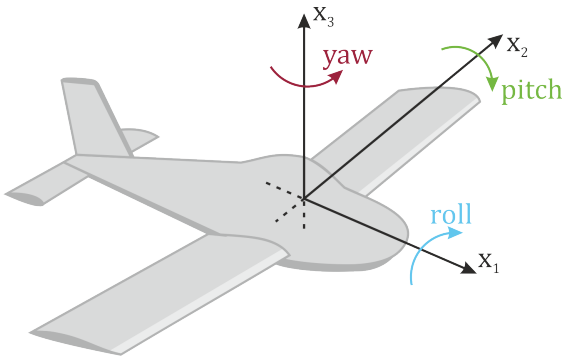

Figure 4.6: Body frame coordinate axes for a fixed-winged UAV body

antenna is assumed to be in the origin. This means the coordinates of the corners of the cuboid are defined within the body frame according to the dimensions. This means, for example, that the coordinates of the front right hand top corner (P_6 in Figure 4.5) can be defined as

$$\mathbf{P}_6 = \left(\frac{length}{2} \quad \frac{width}{2} \quad \frac{height}{2} \right)^T \tag{4.27}$$

and the coordinates of the back left hand bottom corner (P_4) are

$$\mathbf{P}_4 = \begin{pmatrix} -\frac{length}{2} & -\frac{width}{2} & -\frac{height}{2} \end{pmatrix}^T . \tag{4.28}$$

Following (Hofmann-Wellenhof et al. 2003) the dimensions in the direction of across track and height can be derived by rotating the corner points by the attitude parameters roll r, pitch p and yaw y using the rotation matrix $\mathbf{R}$ which reads

$$\mathbf{R} = \begin{bmatrix} \cos p \cdot \cos y & \cos p \cdot \sin y & -\sin p \\ \sin r \cdot \sin p \cdot \cos y & \sin r \cdot \sin p \cdot \sin y & \sin r \cdot \cos p \\ -\cos r \cdot \sin y & +\cos r \cdot \cos y & \\ \cos r \cdot \sin p \cdot \cos y & \cos r \cdot \sin p \cdot \sin y & \cos r \cdot \cos p \\ +\sin r \cdot \sin y & -\sin r \cdot \cos y & \end{bmatrix}^T . \tag{4.29}$$

After rotating the body frame into the local-level frame the height and across track components can be derived. The minimum and maximum deviations of the corner points are then added to the actual deviations of the UAV to the reference trajectory (see Section 5.4).

4.3 Total Deviation

The total deviation includes the actual deviation of the UAV to the reference trajectory, the safety envelope and the protection levels. Compared to the protection levels the safety envelope is small, as can be seen schematically in Figure 4.7. In numbers, this would compare to, for example, approximately 1.5 m for the safety envelope and about 7 m for the protection level in the horizontal plane and in the vertical plane it is around 0.7 m and 14 m. These value are dependent on the application, visible satellites and satellite geometry as well as the dimensions of the used aircraft.

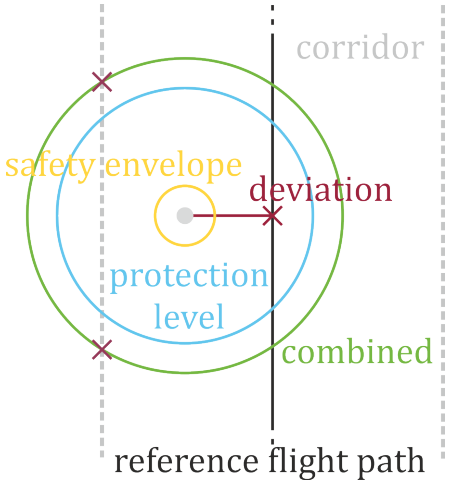

Figure 4.7: Schematic representation of the total deviation

However, both protection levels and safety envelope are needed so the maximum deviation from the defined flight path can be determined. The protection levels define the maximum possible deviation because of various influences (for example, ionospheric delay, clock and orbit errors) whereas the safety envelope accounts for the UAV dimensions instead of only considering the antenna position.

5 Prediction and Detection

In many situations, having knowledge about the future state (for example, the future position or velocity) is useful because it permits one to react accordingly and in a timely manner. This is particularly important for the safe operation of a UAV, including maneuvering beyond line of sight. The prediction of the future position of a UAV can mitigate the risk of leaving the protected airspace.

A safe navigation and piloting of a UAV is almost guaranteed if the aircraft is still located within the protected airspace. Therefore, whether or not the aircraft is located within the protected airspace needs to be determined for the current and predicted future position. The position of the drone, including the calculated protection levels along the trajectory, is identified, which allows for the minimum and maximum deviation of the UAV to the reference flight path to be determined. If the UAV is located outside the flight corridor or will leave the protected airspace while maintaining its direction and motion, a warning (including instructions on how to steer the drone back towards the reference trajectory) will be issued.

For a short period of time, and under the assumption that the current movement will be maintained, the future position of the drone can be determined using a Kalman filter. This is a recursive filter consisting of a measurement update, in which the observations are filtered and corrected, and a time update, in which the future state is calculated based on the current state (Hofmann-Wellenhof et al. 2003). Several (linear) movement models can be used, for example, uniform motion or uniform acceleration. The expected attitude is

determined by using the predicted velocity and acceleration. A regression line was used to predict protection levels.

5.1 Kalman Filter

A Kalman filter is a linear estimation technique for a non-stationary random process. The state vector $\mathbf{x}$ is a function of time. Its basic principle is based on a least squares adjustment, which is a well-known method for estimation of position coordinates, velocity and attitude parameters in navigation if more measurements z_i than unknown parameters x_i exist. This is called an overdetermined equation system. The basic observation equation is defined as

$$\mathbf{z} = \mathbf{H} \cdot \mathbf{x} + \mathbf{v} \ , \tag{5.1}$$

where the design matrix $\mathbf{H}$ defines the linear or linearized relation between the measurements $\mathbf{z}$ and the unknown parameters of the state vector $\mathbf{x}$. The noise vector $\mathbf{v}$, representing the measurement and observation noise, is assumed to follow a Gaussian normal distribution with a zero mean, denoted as $\mathbf{v} \sim N(0, \mathbf{R})$ with $\mathbf{R}$ being its covariance matrix.
Following Hofmann-Wellenhof et al. (2003) the minimization problem $\mathbf{v}^T \cdot \mathbf{R}^{-1} \cdot \mathbf{v} \stackrel{!}{=} \min$ in terms of the best linear unbiased estimate (BLUE), is given as

$$\hat{\mathbf{x}} = (\mathbf{H}^T \cdot \mathbf{R}^{-1} \cdot \mathbf{H})^{-1} \cdot \mathbf{H}^T \cdot \mathbf{R}^{-1} \cdot \mathbf{z} \ , \tag{5.2}$$

where the inverse covariance matrix $\mathbf{R}^{-1}$ is the generalized weight matrix for the observations.
The Kalman filter is best practice if a (discrete) dynamic system is used. This means observations are taken at equally spaced points in time (Kalman 1960), i.e., at discrete time epochs t_k. Therefore, the system is time dependent, which is denoted as $\mathbf{x}(t_k) = \mathbf{x}_k$.

The dynamic behavior describes how the state vector is predicted by the system equations and is defined as

$$\mathbf{x}_k = \mathbf{\Phi}_{k-1} \cdot \mathbf{x}_{k-1} + \mathbf{w}_{k-1} \ , \tag{5.3}$$

where $\mathbf{w}$ is the system noise which describes the uncertainties of modeling the behavior of the dynamic system and which is assumed to follow a Gaussian normal distribution and a zero mean – $\mathbf{w} \sim N(0, \mathbf{Q})$ with $\mathbf{Q}$ being its covariance matrix (Hofmann-Wellenhof et al. 2001). The transition matrix $\mathbf{\Phi}$ represents the linear relation (system equations) between current and predicted parameters.

The estimated state vector $\hat{\mathbf{x}}_{k-1}$ and its covariance matrix $\mathbf{P}_{k-1}$ are changing with time, so they need to be adjusted by using the predictions of $\tilde{\mathbf{x}}_k$ and $\tilde{\mathbf{P}}_k$.

The Kalman filter consists of three main steps which are fed with information from the measurements. In Figure 5.1 this is shown graphically.

Step 1: Gain computation

By comparing the measurement and system noise the Kalman weight (gain) $\mathbf{K}$ is attained.

$$\mathbf{K}_k = \tilde{\mathbf{P}}_k \cdot \mathbf{H}_k^T \cdot (\mathbf{H}_k \cdot \tilde{\mathbf{P}}_k \cdot \mathbf{H}_k^T + \mathbf{R}_k)^{-1} \tag{5.4}$$

Step 2: Measurement update

Predicted values are corrected using new measurements, which are weighted using the Kalman weight.

$$\hat{\mathbf{x}}_k = \hat{\mathbf{x}}_k + \mathbf{K}_k \cdot (\mathbf{z}_k - \mathbf{H}_k \cdot \tilde{\mathbf{x}}_k) \tag{5.5}$$

$$\mathbf{P}_k = (\mathbf{I} - \mathbf{K}_k \cdot \mathbf{H}_k) \cdot \tilde{\mathbf{P}}_k \tag{5.6}$$

Step 3: Time update

As a concept of state transition the prediction of the state vector is calculated by using the transition matrix $\mathbf{\Phi}$. The predicted covariance matrix $\tilde{\mathbf{P}}$ is obtained

by using error propagation of Eq. (5.3).

$$\tilde{\mathbf{x}}_{k+1} = \mathbf{\Phi}_k \cdot \hat{\mathbf{x}}_k \tag{5.7}$$

$$\tilde{\mathbf{P}}_{k+1} = \mathbf{\Phi}_k \cdot \mathbf{P}_k \cdot \mathbf{\Phi}_k^T + \mathbf{Q}_k \tag{5.8}$$

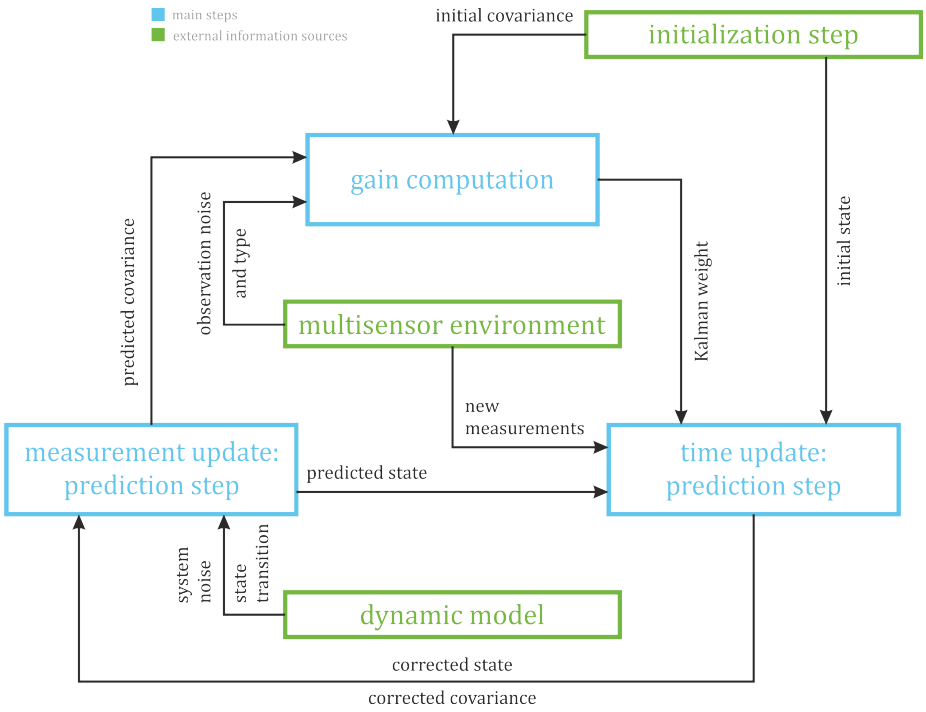

Figure 5.1: Graphical representation of the basic principle of the Kalman filter

The gain matrix gives more weight to either the measurements or the prediction depending on the accuracies of $\mathbf{z}$ or $\tilde{\mathbf{x}}$. If the measurements are very accurate ($\mathbf{R}_k \approx 0$), i.e., the prediction is assumed to have a low accuracy, the gain matrix $\mathbf{K}$ approximately equals the identity matrix ($\mathbf{K}_k \approx \mathbf{I}$). Therefore, the measurements are given more weight ($\hat{\mathbf{x}}_k \approx \mathbf{z}_k$). However, if the measurements are inaccurate, i.e., the prediction is assumed to have a high accuracy ($\tilde{\mathbf{P}}_k \approx 0$), the Kalman weight becomes nearly zero ($\mathbf{K}_k \approx 0$), which means that the dynamic model is heavily weighted ($\hat{\mathbf{x}}_k \approx \tilde{\mathbf{x}}_k$) compared to the new measurements (Hofmann-Wellenhof et al. 2003). Advanced Kalman filtering techniques are used, for example, for multisensor environments or non-linear systems.

5.1.1 Dynamic Models

If a moving object is considered, the state vector can, inter alia, consist of position and velocity, or position, velocity and acceleration, depending on whether it is a uniform moving or uniformly accelerated system (Hofmann-Wellenhof et al. 2001). Since a constant force is rare, the unknowns are affected in either case by a (random) higher derivative of position with respect to time. For velocity, the derivative is acceleration. In the case of acceleration, the third derivative of position with respect to time is called jerk. Higher derivatives are snap, crackle and pop – but no agreement on these names exists (Eager et al. 2016).
The state transition is specified by a system of the first order differential equations of time (Kalman 1960), which are forming the transition matrix $\mathbf{\Phi}$. Assuming uniform movement or acceleration, the system equations for velocity, acceleration and jerk are linear. Using a Kalman filter a prediction can be made for any instant of the time $t_{k+1} = t_k + \Delta t$ (Hofmann-Wellenhof et al. 2001).
For the following dynamic models, it is considered that position x, y and y and velocity $\dot{x}$, $\dot{y}$, $\dot{z}$ are observed at each epoch,

$$\mathbf{z}_k = \begin{pmatrix} x & y & z & \dot{x} & \dot{y} & \dot{z} \end{pmatrix}^T . \tag{5.9}$$

Using error propagation of the observation covariance matrix $\mathbf{R}$ the covariance matrix of the state vector is given by

$$\mathbf{Q}_k = \mathbf{N} \cdot \mathbf{R}_k \cdot \mathbf{N}^T, \tag{5.10}$$

where the matrix $\mathbf{N}$ corresponds to the relation between the observation noise $\mathbf{v}$ and the system noise $\mathbf{w}$, which is dependent on which dynamic model is used. The relation can, for example, be expressed by Eqs. (5.13) and (5.14) as well as Eqs. (5.17) through (5.19).

Uniform Movement

If an object is assumed to be moving with constant velocity, the state vector consists of position and velocity,

$$\mathbf{x}_k = \begin{pmatrix} x & y & z & \dot{x} & \dot{y} & \dot{z} \end{pmatrix}^T . \tag{5.11}$$

Therefore, the system equation equals

$$\mathbf{x}_{k+1} = \begin{pmatrix} x \\ y \\ z \end{pmatrix} + \Delta t \cdot \begin{pmatrix} \dot{x} \\ \dot{y} \\ \dot{z} \end{pmatrix} , \tag{5.12}$$

which is linear, and therefore means that the transition matrix can be derived directly. The velocity is influenced by random acceleration which is applied to $\mathbf{Q}$ by $\mathbf{N}$, which consists of the following equations

$$\mathbf{x} = \frac{1}{2} \cdot \Delta t^2 \cdot \ddot{\mathbf{x}} , \tag{5.13}$$

$$\dot{\mathbf{x}} = \Delta t \cdot \ddot{\mathbf{x}} , \tag{5.14}$$

where the integration interval Δt equals the time between the current and predicted time epoch.

Uniform Acceleration

If a system is uniformly accelerated, the state vector is expanded by the parameters for acceleration:

$$\mathbf{x}_k = \begin{pmatrix} x & y & z & \dot{x} & \dot{y} & \dot{z} & \ddot{x} & \ddot{y} & \ddot{z} \end{pmatrix}^T . \tag{5.15}$$

This means that there is an additional term added in the system equation

$$\mathbf{x}_{k+1} = \begin{pmatrix} x \\ y \\ z \end{pmatrix} + \Delta t \cdot \begin{pmatrix} \dot{x} \\ \dot{y} \\ \dot{z} \end{pmatrix} + \frac{\Delta t^2}{2} \cdot \begin{pmatrix} \ddot{x} \\ \ddot{y} \\ \ddot{z} \end{pmatrix} \ , \tag{5.16}$$

which still is a linear equation and leads directly to the transition matrix. The jerk $\dddot{\mathbf{x}}$ is applied to the covariance matrix. Therefore, $\mathbf{N}$ consists of the following equations:

$$\mathbf{x} = \frac{1}{6} \cdot \Delta t^3 \cdot \dddot{\mathbf{x}} \ , \tag{5.17}$$

$$\dot{\mathbf{x}} = \frac{1}{2} \cdot \Delta t^2 \cdot \dddot{\mathbf{x}} \ , \tag{5.18}$$

$$\ddot{\mathbf{x}} = \Delta t \cdot \dddot{\mathbf{x}} \ . \tag{5.19}$$

In this thesis, a Kalman filter is used to predict the position of the UAV to ensure that the UAV does not leave the protected airspace while maintaining its motion and direction. Therefore, it is not enough to only predict the change between measurement epochs, but it is also necessary to anticipate the position a few seconds ahead. Depending on which one of the investigated dynamic models is used, the statistical values calculated with respect to the filtered trajectory differ. The smaller the prediction time, the closer the statistical values will be to the reference.

In Figure 5.2 and Figure 5.3, the statistical values with reference to the filtered trajectory (prediction time equals the measurement update time of 1 second) are shown graphically. Those values include the minimum and maximum deviation of the predicted positions to the filtered positions. The latter equal the raw observations. The standard deviation is shown as an interval. The dynamic system noise is set empirically depending on application, for a car with 1 $\mathrm{m/s^3}$ and for an ultra light aircraft with 3 $\mathrm{m/s^3}$. Even though the standard deviations of both dynamic models are close, only a prediction time up to

5 seconds (depending on the application and aircraft characteristics) is suitable because the maximum and minimum are within the order of magnitude of the calculated protection levels (see Section 4.1).

A prediction of 10 seconds would allow the pilot to react in accordance with the situation and in a timely manner. However, the deviations from the filtered position values for this prediction time are too large to be of benefit because a flying UAV is a fast changing dynamic system. Therefore, a shorter interval is recommended because the smaller the time interval for the prediction, the smaller the deviations will be. Up until a prediction step of 5 seconds, both dynamic models are applicable, but the uniform acceleration model shows bigger deviations for greater intervals. This is because the uniform acceleration model reacts stronger to slight changes in movement.

The differences between the filtered and predicted coordinates X, Y, Z are shown in Figure 5.4, where it can be seen, that a big deviation of the predicted position takes a short period to recover. In average, the differences are around 1 cm. Even though the maximum differences are approximately ± 15 m, the prediction accuracy is sufficient because it only gives an impression where the UAV could be located in the future while maintaining motion and direction.

A UAV is closest to a uniformly accelerated system because the aircraft needs constant acceleration to fly (i.e., thrust). Therefore, the uniform acceleration model is better fitting to describe the motion. Accordingly, a prediction time of maximum 5 seconds should be used, where the deviations from the filtered trajectory are within the dimension of the protection levels. A reaction time of approximately 5 seconds for the pilot is assumed to still be enough time to ensure an appropriate response if the aircraft is predicted to leave the protected airspace.

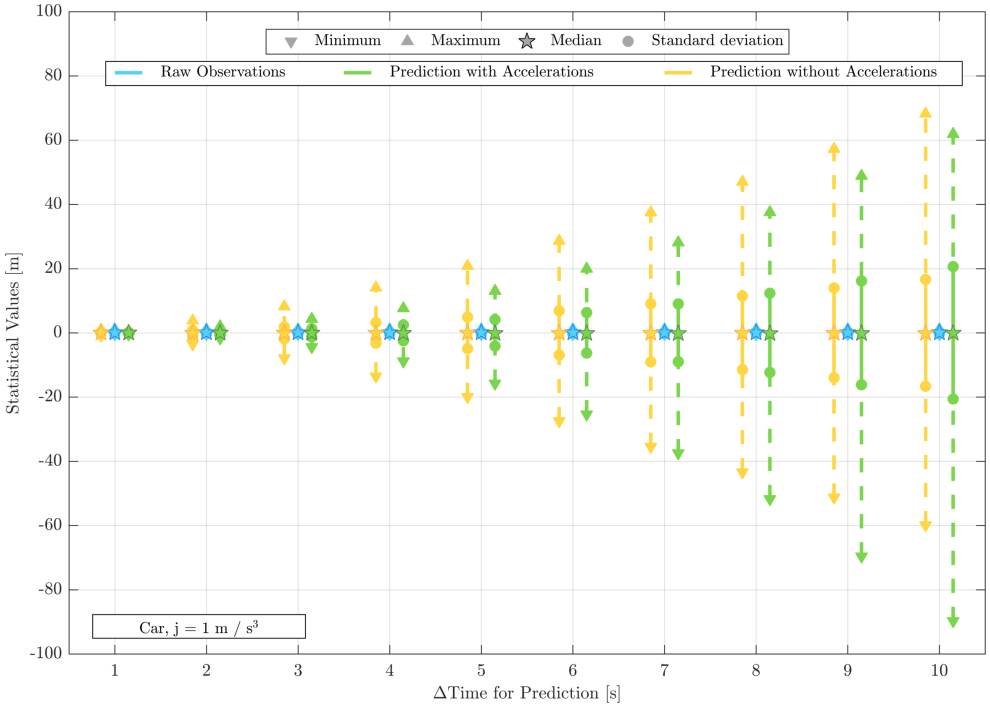

Figure 5.2: Statistical values of the prediction with respect to the filtered trajectory (car)

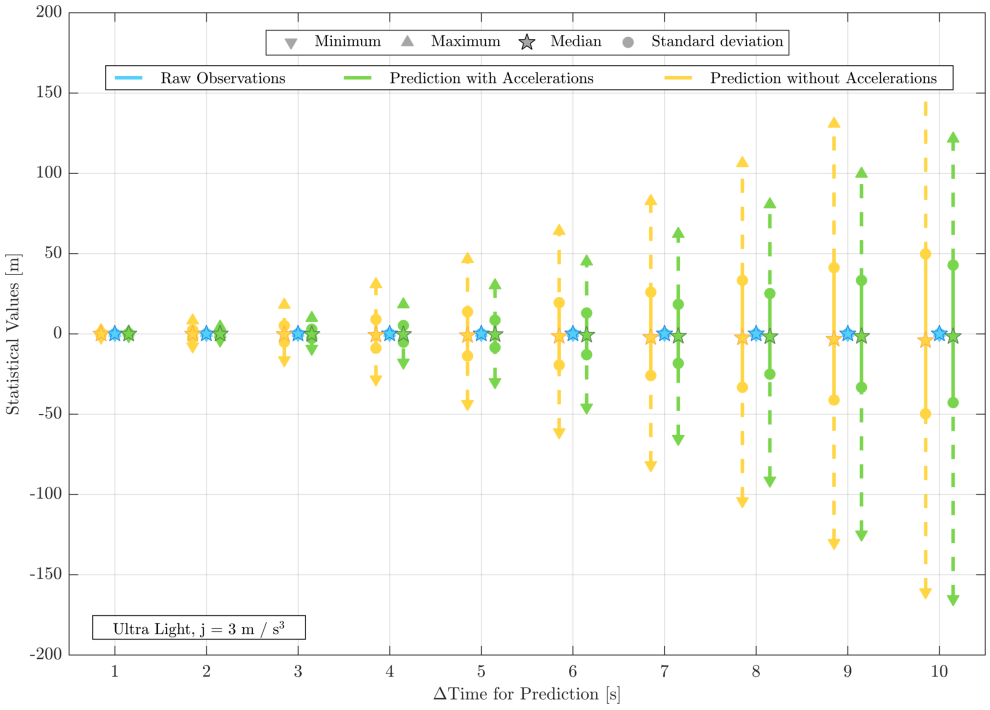

Figure 5.3: Statistical values of the prediction with respect to the filtered trajectory (ultra light aircraft)

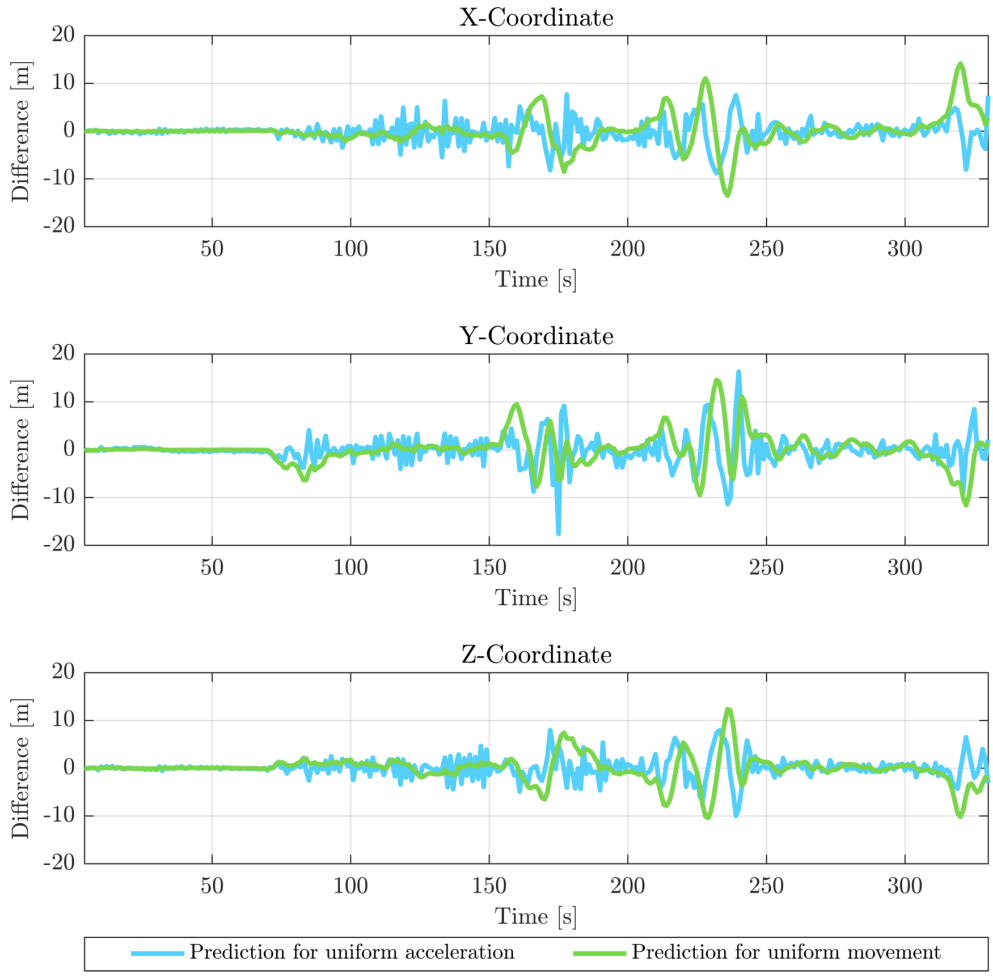

Figure 5.4: Differences of predicted coordinates to filtered coordinates ($\Delta t_{=}$ 4 seconds)

5.2 Prediction of Attitude

The attitude parameters roll (bank) r, pitch p and yaw (heading) y are needed for the safety envelope calculation (described in Section 4.2). Predicting these values within the Kalman filter would result in using an advanced Kalman filter, i.e., becoming an iterative procedure because of the (partly) uncorrelated character of the attitude (Hofmann-Wellenhof et al. 2003). Another possibility is to calculate the attitude using already predicted values. This is accomplished by using the angular velocity ω, which describes the rate of change in orientation. The components of the angular velocity vector $\boldsymbol{\omega}$ in the body frame correspond to the attitude parameters r, p and y. According to Polychronopoulos et al. (2007), the

angular velocity vector can be computed using the velocity vector $\dot{\mathbf{x}}$ and acceleration vector $\ddot{\mathbf{x}}$, both rotated to the local-level frame using Eq. (3.7), which is denoted with the index l:

$$\boldsymbol{\omega} = \frac{(\dot{\mathbf{x}}_l \times \ddot{\mathbf{x}}_l)}{\|\dot{\mathbf{x}}_\mathbf{l}\|^2} \ . \tag{5.20}$$

Roll and pitch can be derived directly from $\boldsymbol{\omega}$, the heading y in the horizontal plane is calculated using the East and North components of the velocity vector (Koppert 2015), which reads

$$\tan y = \frac{\dot{x}_E}{\dot{x}_N} \ . \tag{5.21}$$

Eqs. (5.20) and (5.21) are an option to estimate the attitude parameters in the future because the predicted values for velocity and acceleration are used. Since those parameters are only applied for the calculation of the (future) safety envelope, a highly accurate prediction is not needed because – as mentioned – the prediction only gives an impression of where the UAV will be located.

Figure 5.5 shows the differences between predicted and actual attitude. The predicted values for roll and pitch match the actual attitude parameters except for a time offset. This is because the prediction of the velocity and acceleration within the Kalman filter uses current parameters and does not foresee any change in attitude or direction. Therefore, any change is only estimated and predicted as soon as an actual change happens, which means that if there is any variation in velocity and acceleration, the attitude parameters show a change as well. This can particularly be seen in the values of the heading. The higher differences in the heading are a result of Eq. (5.21) where the East and North components of the state vector are used. If, for example, a turn is performed then there is a constant change in the coordinates, which leads to a change in the heading as well. However, the

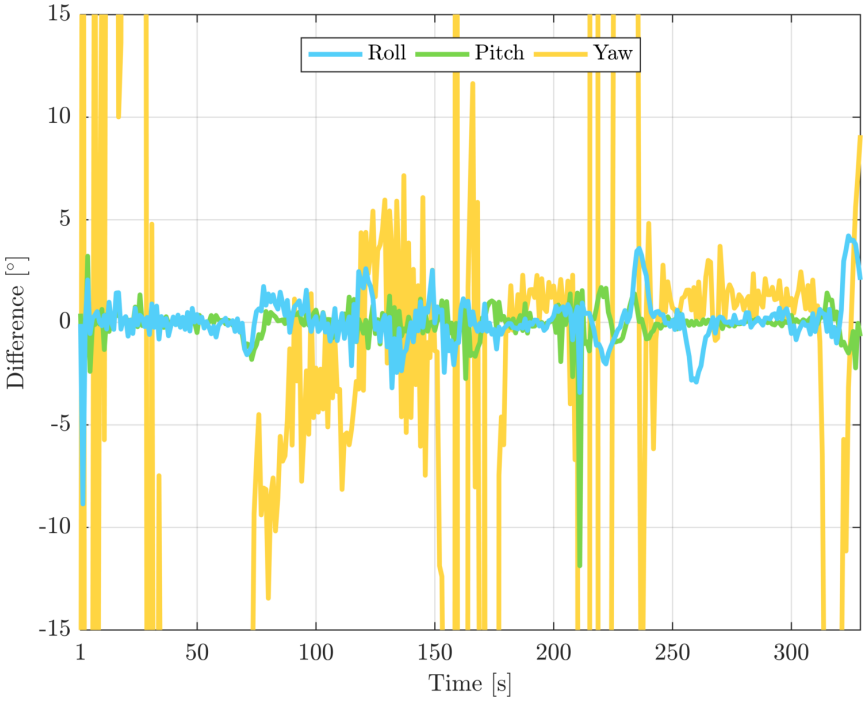

Figure 5.5: Differences of predicted to actual attitude parameters ($\Delta t = 4$ seconds)

filter assumes, for its prediction step, that the motion and direction are not changing, and this can be seen in the higher differences of the heading, especially during turns.

5.3 Prediction of Protection Levels

Because protection levels do not change in average more than around 15 cm horizontally and vertically within 10 seconds, the prediction using a Kalman filter would not have a big benefit. However, since they are not constant over time, a prediction with a regression line can be used. This is accomplished by using a least squares adjustment with the linear equation

$$y = a \cdot x + b \tag{5.22}$$

as the observation equation for a linear regression line, where a describes the slope and b expresses the point at which the line crosses the y-axis. Since a linear regression line might not be fitting, also a quadratic regression line using

$$y = a \cdot x^2 + b \cdot x + c \tag{5.23}$$

as the observation equation, with a, b and c being arbitrary constants, which need to be estimated using the least squares adjustment, can be used. This is also the case for a cubic regression line with the additional arbitrary constant d in the observation equation

$$y = a \cdot x^3 + b \cdot x^2 + c \cdot x + d \ . \tag{5.24}$$

There are almost no differences between the different regression lines. All of the different regression lines fit each horizontal and vertical protection levels.
However, since protection levels oscillate over time – resulting from the usage of the transmission time of the SBAS messages, which changes every second – a low pass filter is used to smooth the protection levels before the least squares adjustment. This filter needs a transient time at the beginning. The filtered values are used to calculate the regression lines except during this transient time in which the actual protection levels are used. During this time, especially the cubic regression line is overshooting the actual protection levels.
In Figure 5.6, the predicted values are shifted in time. This is a result of the filter delay and the added prediction time. The smallest differences between actual and predicted values are achieved when using a linear regression line. It is expected that the protection levels follow a linear behavior – except for a few outliers – and therefore the linear regression line is the best fit.

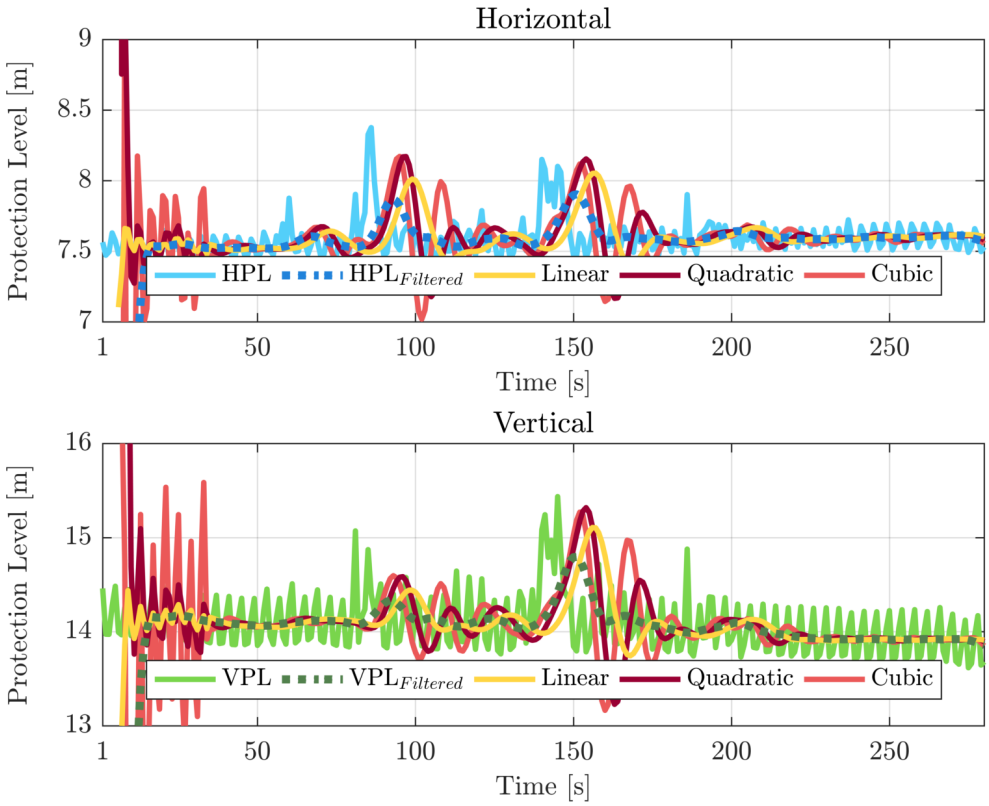

Figure 5.6: Fitted predicted regression lines to filtered protection levels (horizontal and vertical)

5.4 Detection and Alarming

To determine if the UAV is still located within the protected airspace, the deviations in height and across track (described in Section 3.4) are compared with the maximum allowed deviations. The corridor is defined as an ellipse, whose semiaxes equal the maximum allowed deviations in height and across track and whose center is at the intersection point. The radius of the ellipse at the angle α – the direction to the position of the UAV – is basically compared with the length of the difference vector between the intersection point at the reference trajectory and the position of the aircraft. This is schematically presented in Figure 5.7.

However, this length is not adjusted for the protection levels and the dimensions of the safety envelope. For this reason, a second ellipse is calculated, of which the length of the

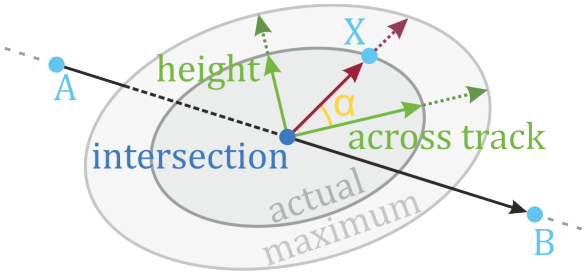

Figure 5.7: Schematic representation of ellipse semiaxes representing flight corridor

semiaxes equal the deviations in height and across track, including the applied protection levels and safety envelope. The radius of this ellipse at the angle α is then compared with the radius of the ellipse of the maximum deviations. If the latter is exceeded, the UAV is no longer located inside the protected airspace. In the case of the predicted position, it means that the UAV will leave the defined corridor in the future if maintaining heading and motion. In any of those cases, a warning – including a possible direction to steer the aircraft back into the protected airspace – is issued to the pilot. A possible realization of such a flight monitor is shown in Figure 5.8.

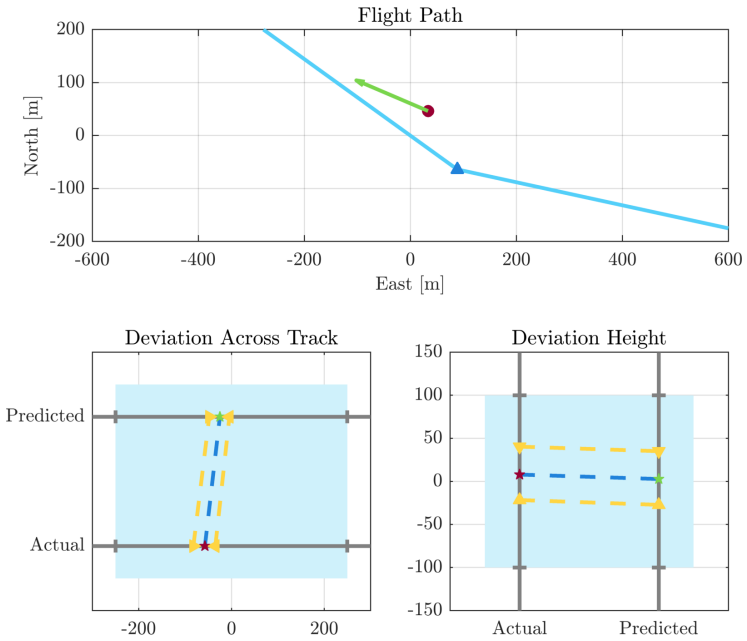

Figure 5.8: Possible realization of a flight monitor showing actual and predicted deviations

The horizontal protection level is defined as the radius of a circle in the horizontal plane (RTCA 1999), as described in Section 4.1. Accordingly, the position also shows deviations in the along track direction. Therefore, the horizontal protection levels are applied to the along track component of the position in and against the direction of flight. This leads to two possible positions for which the deviations to the reference trajectory are calculated and compared to the maximum allowed deviations. This results in minimum and maximum possible deviations, which are also shown in the flight monitor in Figure 5.8. The "true" deviation is within this area. The pilot is warned in any case, for example, if only the maximum deviation lies outside of the defined corridor, as can be seen in Figure 5.9.

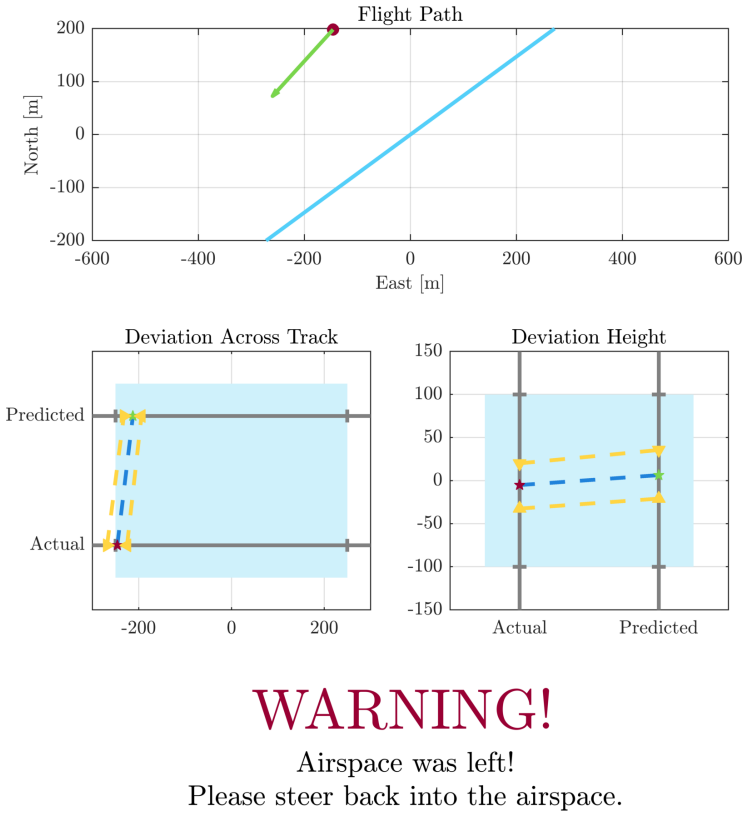

Figure 5.9: Flight monitor showing a warning that the protected airspace was left

6 Results

First simulations, made using data from a test drive with a car, were already showing promising results. However, because an aircraft in flight behaves differently than a car on paved roads, a test flight using an ultra light aircraft was conducted to gather further test data.

Measurement data is recorded in real-time and referenced by UTC in seconds. The data set consists of satellite dependent data including among others the PRN, elevation, azimuth and pseudorange measurements and the C/N0 for each tracked satellite (GPS and Galileo). Further included is the state data with position, velocity and attitude of the receiver for each epoch including their standard deviations and the covariance matrix. And last the raw bits of the Galileo navigation message and the SBAS messages are transmitted. Measurement data for the test drive and test flight was evaluated in post-processing.

6.1 Test Drive

The test drive was conducted on 11 July 2017 in Kalsdorf bei Graz, Austria. The total drive time was around 5 minutes, starting at 08:50 UTC. The maximum allowed deviations from the reference trajectory in across track and height were set to 25 m each. These are composed of the magnitude of the calculated horizontal and vertical protection levels (max. 15 m and max. 20 m) and the mean width of the road (10 m) and the height changes along the path (10 m) respectively.

6.1.1 Trajectory

In post-processing the waypoints for the trajectory were defined, whose coordinates are listed in Table 6.1. If a waypoint is defined as a fly-by waypoint, turn points are calculated, which are also used to describe the turn area of that waypoint. In Figure 6.1 part of the

Table 6.1: Waypoints for the test drive's theoretical flight path

Waypoint Number	φ [°]	λ [°]	**Height** [m]	**fly-over/ fly-by**
1	46.978468	15.449075	375.3	fly-over
2	46.977659	15.451395	374.9	fly-over
3	46.976243	15.453917	373.6	fly-over
4	46.975251	15.455871	373.5	fly-over
2	46.974381	15.457353	374.5	fly-by
3	46.973755	15.457331	373.6	fly-by
4	46.973786	15.457717	373.6	fly-by
5	46.969944	15.459556	374.0	fly-by
6	46.965688	15.446746	373.0	fly-by
7	46.966332	15.446778	373.0	fly-over

reference trajectory with its waypoints and turn points is shown and includes the filtered trajectory (driven path) and the predicted path. The prediction time $\Delta t_{prediction}$ was set to 4 seconds. It can be seen that the filtered trajectory mostly follows the reference flight path and even though the deviations of the predicted trajectory to the reference flight path are bigger, they still lie within the corridor in the horizontal plane. The biggest differences between the predicted and actual flight path can be seen during turns. However, this is considered by expanding the corridor by the transition area when a fly-by turn is carried out.

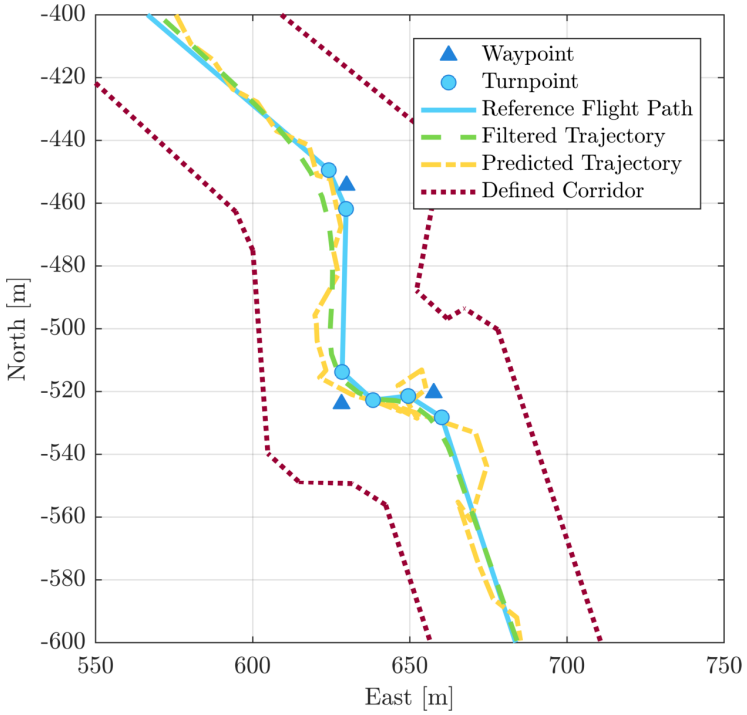

Figure 6.1: Theoretical, filtered and predicted trajectory of the test drive

6.1.2 Deviations

The mean horizontal protection level is 8.06 m, the mean vertical protection level is 14.53 m. The calculated safety envelope's average dimensions are in across track around 1.30 m and in height about 0.73 m. Those values are added to the actual deviations. The total (minimum and maximum) deviations are shown in Figure 6.2. In the instances where the predicted values are not seen, they lie behind the actual deviations, and therefore they have a lower or equal order of magnitude. At the beginning of the trajectory, the road makes two wide turns, which are defined by fly-over waypoints. However, that these waypoints are not perfectly modeling the driven path, can be seen in Figure 6.2 in the across track deviations between 100 seconds and 150 seconds.

Except in two cases, neither the filtered trajectory nor the predicted path left the virtual protected airspace (defined corridor) during the drive along the planned trajectory. The

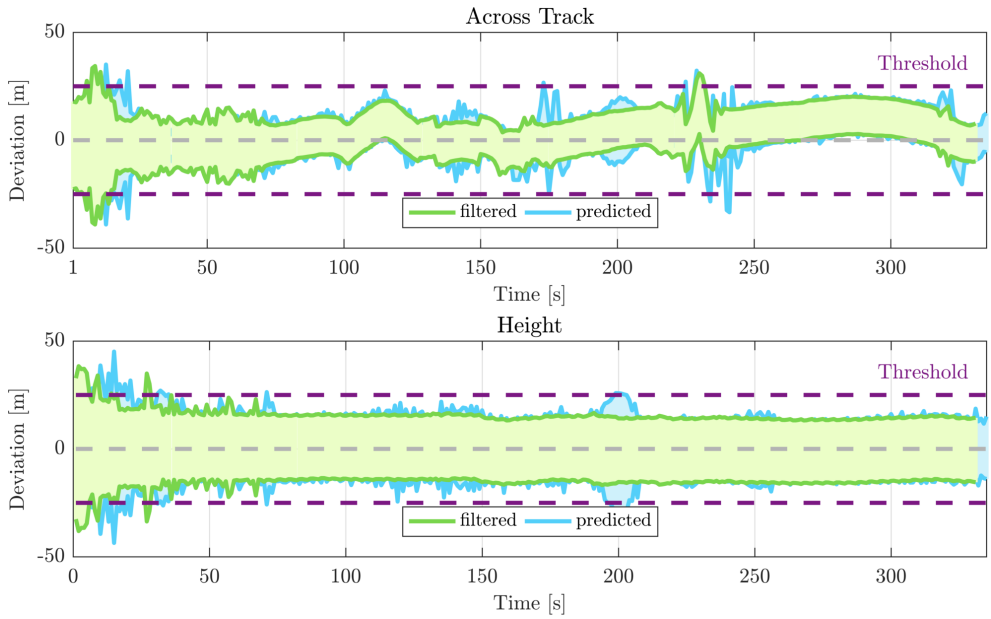

Figure 6.2: Deviations in across track and height for the test drive

corridor was left during the initialization period in the beginning – because no detection of static epochs is implemented in the Kalman Filter – and at the roundabout when instead of performing the planned right turn, a whole round was driven. In Figure 6.3 the trajectory and the deviations during the drive in the roundabout are shown.

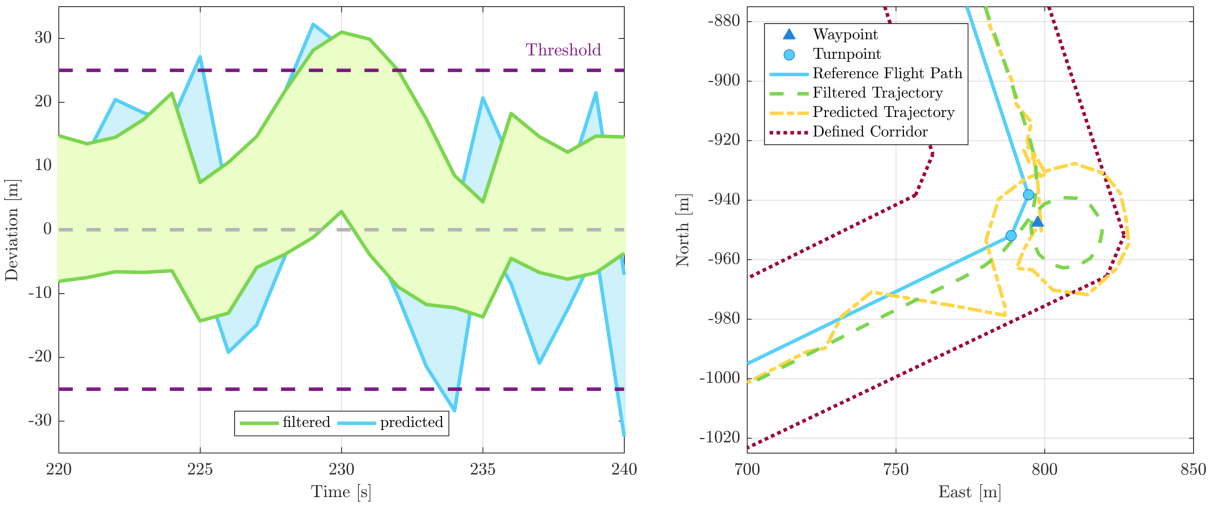

(a) Deviation in across track (b) Filtered and predicted trajectory

Figure 6.3: Trajectory and deviations in across for the drive in the roundabout

Altogether, the algorithm promised good results. However, a car's attitude in roll and pitch are not supposed to change and there is no (flying) altitude to consider, thus further testing with data from an actual flight was needed.

6.2 Test Flight

A test flight with the ultra light aircraft Ikarus C42 was performed on 20 December 2017, with take-off from the aerodrome in Weiz, Austria (LOGW) at 14:28 UTC. The aircraft – shown in Figure 6.4 – was equipped with two IMUs and a GNSS receiver (able to process GPS as well as Galileo), as can be seen in Figure 6.5. The IMUs and the GNSS antenna were placed in the cockpit, the receiver and the data drives were located in the back. The test flight was a joint action of the FH Joanneum, Institute of Geodesy at Graz University of Technology, Igaspin and TeleConsult Austria.

Figure 6.4: Ultra light aircraft Ikarus C42

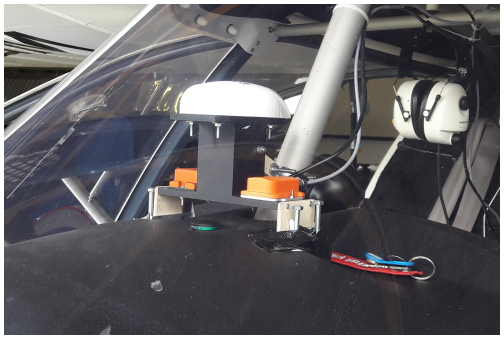

(a) GNSS antenna and two IMUs

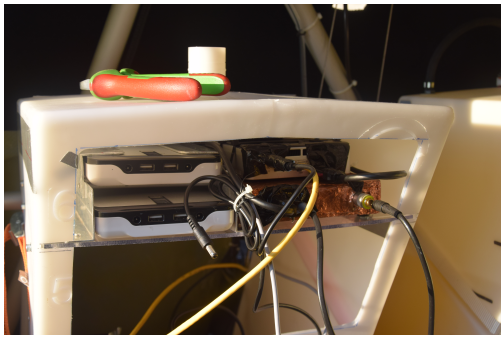

(b) GNSS receiver

Figure 6.5: Equipment onboard the ultra light aircraft

6.2.1 Pre-Flight Tasks

The planned reference flight path consists of fly-by and fly-over waypoints. The trajectory was planned so that some acute angles and some obtuse angles as well as a right angle are flown. According to RTCA (1999), waypoints with an angle greater than 120° are supposed to be treated as fly-over waypoints. In Table 6.2 the waypoints are listed. In this case a constant flying altitude of 3100 ft (around 945 m above ground) is assumed for all waypoints.

Table 6.2: Waypoints for the test flight's reference flight path

Waypoint Number	φ [°]	λ [°]	**Height** [m]	**fly-over/ fly-by**
1	47.141900	15.845600	945	fly-over
2	47.152526	15.847910	945	fly-by
3	47.162944	15.886165	945	fly-by
4	47.145757	15.906720	945	fly-over
5	47.121526	15.907594	945	fly-by
6	47.120045	15.938942	945	fly-over
7	47.111647	15.956792	945	fly-by
8	47.093167	15.919963	945	fly-by
9	47.102242	15.858936	945	fly-over
10	47.112044	15.839039	945	fly-over
11	47.132724	15.843479	945	fly-over

In Figure 6.6 the reference flight path is shown graphically. Turn points were calculated based on a nominal bank angle of 15° and a nominal ground speed of 68 kn (approximately 35 m/s or 126 km/h) – based on observations of the prior flight on 19 December 2017. During that flight, without any measurement equipment onboard, the designed trajectory was tested.

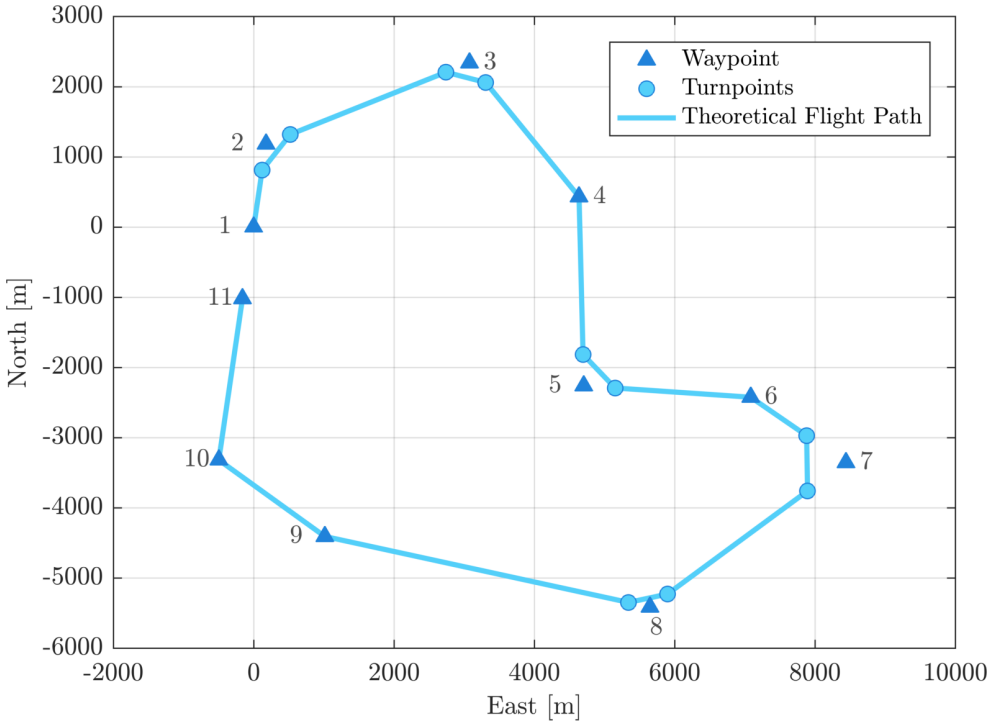

Figure 6.6: Theoretical flight path based on waypoints planned for test flight

The original trajectory consisted of an additional loop at the end, which can be seen in the tracked trajectory in Figure 6.7. This loop was not flown during the actual test flight due to time limitations for a visual flight rules (VFR) flight because of the sun set.

The trajectory was flown twice in the course of the actual test flight carrying the measurement equipment on 20 December 2017. The first round was supposed to be followed exactly, this means, for example, no missed points and only straight lines between waypoints. Whereas the second round should be flown messy, for example, not keeping the altitude or missing fly-over waypoints. Due to an unknown error, data was only recorded

from the start to approximately the middle of the second round – which still provides enough data to be processed and analyzed.

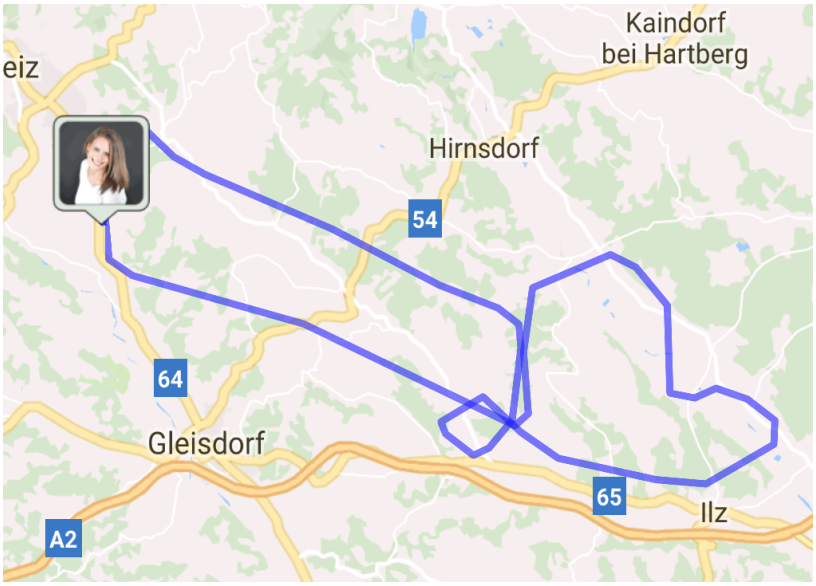

Figure 6.7: Tracked trajectory flown on 19 December 2017 overlaid with Google™ Maps

Lever Arm Measurements

Pre-flight the lever arm between the antenna and the body frame origin needed to be determined. The lever arm measurements were conducted together with the Institute of Geodesy at Graz University of Technology. Therefore, the dimensions of the aircraft were measured using a total station. In Figure 6.8 the measurement set-up can be seen. From one stand point the aircraft (nose, tail, wing tips and height) and the antenna position were measured in a local-level frame with its origin at the position of the total station.
The dimensions of the aircraft are:

- Width: 6.34 m (wingspan)
- Length: 9.42 m (nose to tail)
- Height: 1.83 m (wheels to top)

(a) Total station (b) Position related to the aircraft

Figure 6.8: Set-up for lever-arm measurements

6.2.2 Post-Flight Analysis

The margin of the protected airspace was set the same for both rounds even though the test data for each round was evaluated separately. The magnitude of the protection levels including the average dimensions of the aircraft contributing to the safety envelope (in across track around 3.09 m, in height around 1.16 m) was the same in both cases. A prediction time $\Delta t_{prediction}$ of 4 seconds was chosen. The average standard deviation for the 3D position for the total flight time equals 1.04 m – which amounts to a horizontal position error of 0.73 m and a standard deviation in height of 0.74 m. In Figure 6.9 the flown flight path for Round 1 and Round 2 are shown together with the reference trajectory, where the differences between Round 1 and Round 2 can be seen.

Size of Protected Airspace

The protected airspace in the horizontal and vertical plane was set according to a certain tolerance, the magnitude of the protection levels and an additional buffer to account for variables such as for wind gusts and thermal currents. For the vertical limits a tolerance of ±150 ft (around 45 m) was chosen, together with the average magnitude of the vertical protection levels of around 30 m and an additional safety buffer of 25 m, this results in a maximum allowed deviation in height of 100 m. In the horizontal plane a tolerance of ±5° (equal to around 175 m at 2 km) has been accepted. Including the magnitude

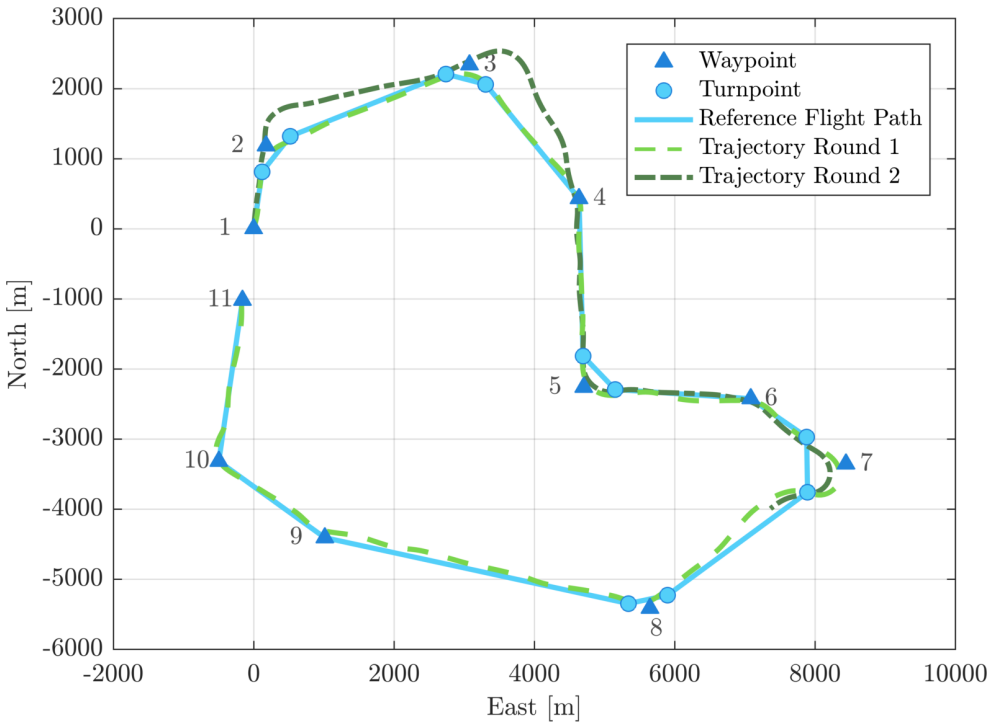

Figure 6.9: Flown track in Round 1 and Round 2

of the horizontal protection level of around 20 m and the additional buffer of 55 m, the maximum allowed deviation in across track equals 250 m. In addition, in the case of fly-by waypoints, the corridor is extended for the transition area (described in Section 3.3). Using those corridor limits, the protected airspace was left in Round 1 only 1.55 % of the time versus a predicted leaving of 1.70 %. Whenever the corridor was actually left, it was predicted as well. This shows that chosen margins of the corridor were suitable for this application.

Dilution of Precision

The magnitude of the protection levels was the same in both rounds. The horizontal protection levels are around 17.85 m and the average vertical protection levels are 27.45 m. Those protection levels are higher than calculated in Section 6.1.2. A reason for this could be the mounting of the antenna. Its position inside the cockpit not only resulted in a higher C/N0, which increases the variance of the airborne receiver error, but also shaded

the signals coming from behind the aircraft. This may have caused a poor geometry of the visible satellites – a measure for this is the dilution of precision, which is calculated using the cofactor matrix of the parameters $\mathbf{Q}_x$. The usual factors for position dilution of precision (PDOP), horizontal dilution of precision (HDOP) and vertical dilution of precision (VDOP) for six to twelve visible satellites according to Hofmann-Wellenhof et al. (2008) are listed in Table 6.3, together with the calculated factors for the test flight as well as for the test drive.

Table 6.3: Dilution of precision for test flight and test drive

Application	**PDOP**	**HDOP**	**VDOP**	**Visible Satellites**
Nominal	1.1 – 2.9	0.6 – 1.3	0.8 – 2.6	6 – 12
Test drive	2.2	1.7	1.4	9
Test flight	3.0	2.6	1.6	6

During the test drive nine GPS satellites were tracked, during the test flight only six. It can be seen that the values for the test flight are higher than for the test drive. This means the protection levels are higher as well because they are calculated based on the elevation and azimuth between user and each tracked satellite. A skyplot for the visible GPS satellites during the test flight can be seen in Figure 6.10.

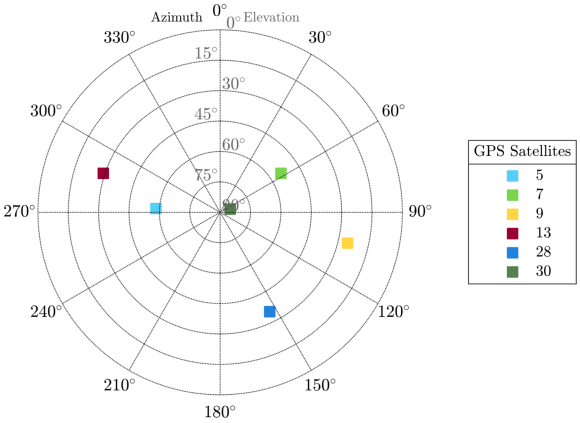

Figure 6.10: Skyplot for visible GPS satellites during test flight

Only a maximum of three Galileo satellites were tracked, which is not enough to calculate

Galileo-based protection levels. The low number of tracked satellites is not only due to the antenna mounting and therefore the signal shading but also because of the available number of Galileo satellites. As of December 2017, there are in total 20 Galileo satellites in orbit, however, two of them are in a non-nominal orbit and four are currently being commissioned given their launch date of 12 December 2017. Consequently, Galileo measurements were only considered for positioning.

Attitude

The test drive – described in Section 6.1 – promised good results for constant attitude in roll and pitch. The analysis of the data from the test flight showed that a changing roll and a changing pitch can be predicted and that a calculation of the safety envelope is possible.

Deviations

During Round 1 the corridor was left for a total of 10 seconds – most after the very acute angle at waypoint #7. Even though the turn transition area is quite big, after the actual turn the aircraft needs extra time and distance to get back to the actual course, which is shown in Figure 6.11. This indicates that the (already larger) corridor around a fly-by waypoint should be enlarged further if an acute angle is supposed to be flown. The positive outcome is that the filtered and predicted flight path match each other well. Note that even though it was detected that the protected airspace was left, the flight paths in Figure 6.11 does not exceed the defined corridor because the path is only shown in 2D and without the safety envelope.

Other than that short period, the aircraft stays inside the corridor. This can also be seen in the deviations in Figure 6.12. Both across track and height are within the defined threshold and predicted and actual deviations in across track are almost the same. This means that the prediction time of $\Delta t_{prediction} = 4$ seconds is suitable. Even though the predicted vertical values are slightly bigger than the actual ones, they still provide a good

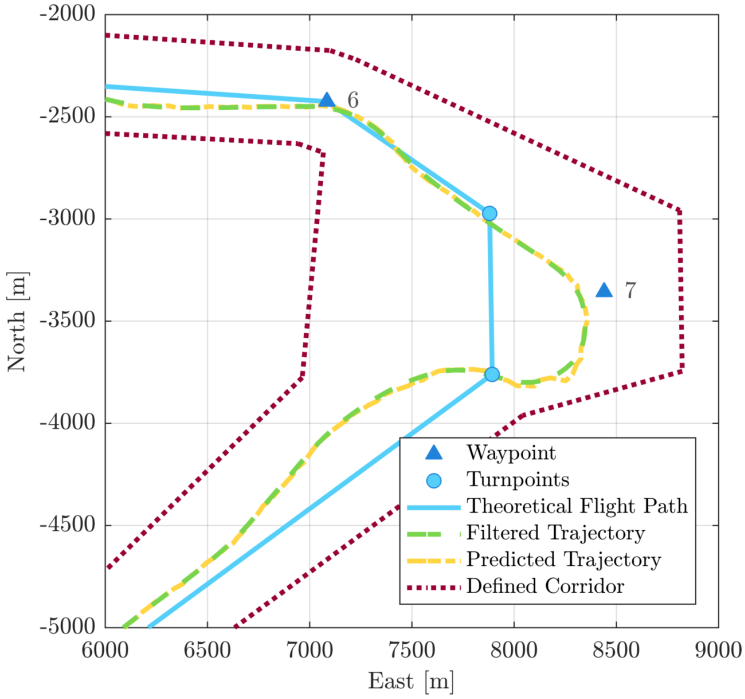

Figure 6.11: Actual and predicted flight path at an acute angle

impression of the predicted deviations.

However, even though in Round 2 predicted and actual values match, they often do not lie within the threshold (actual: 25.46 %, predicted: 28.38 %) – both in across track and height, as shown in Figure 6.13. Since the task of Round 2 was to deliberately deviate from the trajectory, Round 2 can be called successful given each leaving of the corridor was detected by the algorithm.

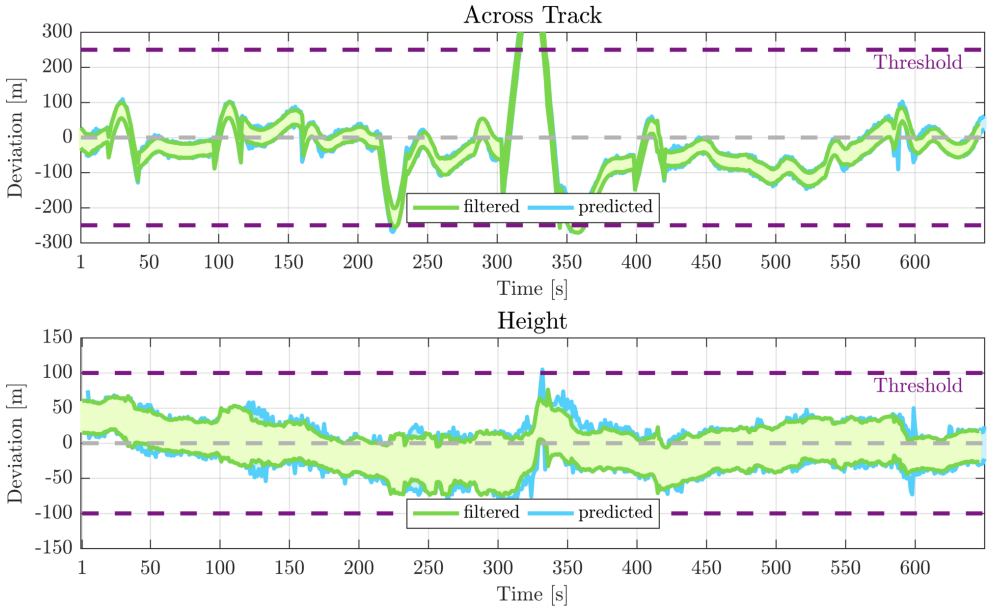

Figure 6.12: Deviations in across track and height for the test flight (Round 1)

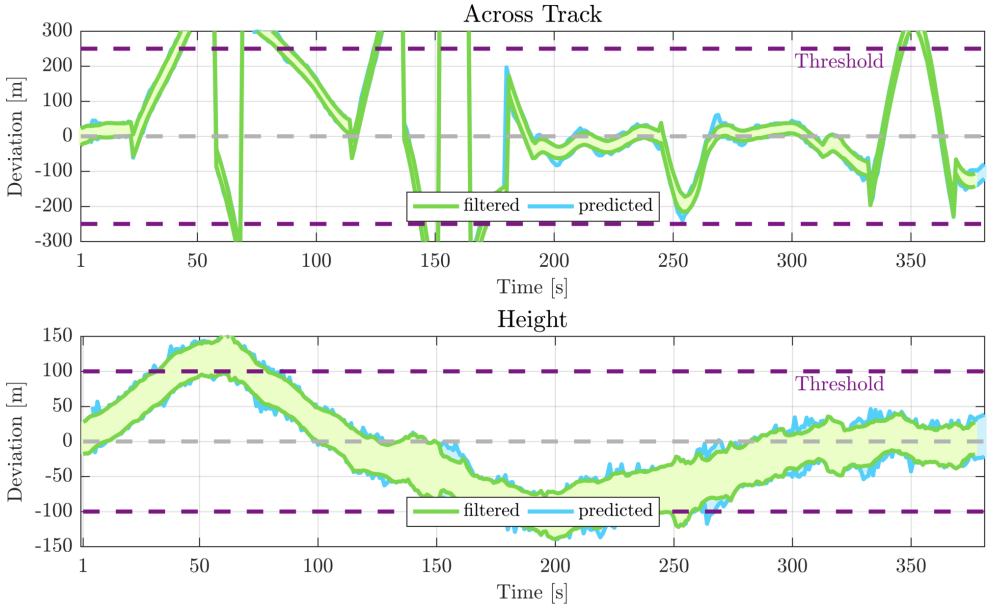

Figure 6.13: Deviations in across track and height for the test flight (Round 2)

7 Conclusions and Outlook

This thesis focuses on establishing a protected airspace for UAVs by defining a reference trajectory using waypoints. The waypoints are defined as either fly-by or fly-over waypoints. This means that the latter are overflown directly whereas turn points are calculated for fly-by waypoints since they are passed within a transition area. The protected airspace itself can be described as a corridor around the reference flight path. The corridor is defined as an ellipse, whose semiaxes equal the maximum allowed deviations in across track and height. The position and attitude of the UAV are determined using a software-based GNSS-receiver and two IMUs. To detect if the UAV is still located within the protected airspace, the position of the UAV with respect to the reference trajectory is determined. This task is accomplished by calculating an intersection point along the defined flight path. The difference vector between the UAV position and the intersection point is then split into its horizontal (across track) and vertical (height) components. A safety envelope, which consists of the dimensions of the UAV and the calculated protection levels is added to the actual deviations. Horizontal and vertical protection levels are a measure for the trust that can be put into the correctness of the position solution and are part of the integrity concept. They are calculated based on data transmitted via SBAS messages. To account for the whole UAV and not only for the position of the antenna, the UAV's dimensions according to its attitude in the horizontal and vertical plane are determined. The total deviations are then compared with the maximum allowed deviations of the protected airspace – if those are exceeded, a warning to the pilot will be issued. To anticipate if the UAV will leave the

protected airspace in the future while maintaining the current movement and heading, a Kalman filter is used to predict the UAV position. In addition protection levels and the attitude parameters are predicted as well.

The developed algorithm is designed using current standards in aviation and providing a solution to safely maneuver a UAV beyond line of sight. Predicting the future UAV position is a tool to enhance safety when the aircraft can not be seen from the ground control station because it helps to separate air traffic and maneuver UAVs within a specified and safe environment, for example, over non-heavily populated areas. Typically, the calculation of the protection levels using data from SBAS messages is only possible for GPS. However, this thesis provides a possibility to also determine Galileo-based protection levels using SISA, which is transmitted with the Galileo navigation message. In addition, this calculation could also be used for a combined Galileo-based and SBAS-based protection level solution. Nevertheless, a future modification of the calculation of protection levels for multi-frequencies, by scaling the variance of the ionospheric delay, is suggested. Using a safety envelope, which includes the dimensions of the UAV, can be important for bigger drones, for example, with a wingspan in the magnitude of the protection levels. First tests have already shown promising results. Not only was it detected when the protected airspace was left, but it was also be predicted. A prediction time $\Delta t_{prediction}$ of 4 seconds as well as the magnitude of the maximum allowed deviations proved to be appropriate for this application. To date, the algorithm has only been tested with a more or less constant altitude. Therefore, further tests including take-off and landing are required.

The algorithm is working as expected and providing good accuracy. However, the current algorithm is only designed for post-processing. In future an adaption to real-time is recommended and needed. To be successful it will be essential to input the pre-planned flight path as reference (for example, by entering waypoint coordinates and definition as fly-by or fly-over waypoints). In addition, an interface for the real-time output is needed as well as the ability to calculate turn points according to the actual ground speed and bank angle

instead of using nominal values. Nevertheless, this algorithm provides a concept for an operational framework for Class 2 UAV operations.

During the course of this thesis two research papers concerning the topic were published at the International Symposium on Precision Approach and Performance Based Navigation (ISPA) in Munich (08 – 09 November 2017) and at the AHORN 2017 in Schladming (23 – 24 November 2017). The related research project DEMONA is funded within the TAKE OFF program of the BMVIT and is managed by the FFG. This developed algorithm allows the safe operation of UAV beyond line of sight by defining a protected airspace and by determining and predicting whether its position is located inside or outside the threshold.

List of Figures

List of Tables

References

Ambrosino G, Ariola M, Ciniglio U, Corraro F, Pironti A, Virgilio M (2006): Algorithms for 3D UAV Path Generation and Tracking. In: Proceedings of the 45$^{\text{th}}$ IEEE Conference on Decision and Control, San Diego, California, December 13 – 15: 5275 – 5280.

Austro Control GmbH (2017): AIP Austria / Luftfahrthandbuch Österreich. Available at `http://eaip.austrocontrol.at`.

Bartolomé JP, Maufroid X, Fernández I, López Salvedo JA, Granados GS (2015): Overview of Galileo System. In: Nurmi J, Lohan ES, Sand S, Hurskainen H (eds.), GALILEO Positioning Technology, Springer, The Netherlands, vol. 182 of Signals and Communication Technology.

BBC News (2017): Drone causes Gatwick Airport disruption. Available at `www.bbc.com/news/uk-40476264#`, (03 July 2017).

Berglez P (2013): Development of a multi-frequency software-based GNSS receiver. PhD dissertation, Institute of Navigation, Graz University of Technology, Austria.

Bundesministerium für Verkehr, Innovation und Technologie (2017): Aviation. `www.bmvit.gv.at/en/verkehr/aviation/index.html`, (October 2017).

Conley R, Cosentino R, Hegarty CJ, Kaplan ED, Leva JL, Uijt de Haag M, Dyke KV (2006): Performance of Stand-Alone GPS. In: Kaplan ED, Hegarty CJ (eds.), Understanding GPS: Principles and Applications, 2$^{\text{nd}}$ edition, Artech House, Norwood.

References

Die Presse (2015): Kamera-Drohne kracht knapp hinter Hirscher auf die Piste. Available at http://diepresse.com/home/sport/wintersport/4893003/KameraDrohne-krachte-knapp-hinter-Hirscher-auf-die-Piste, (23 December 2015).

Eager D, Pendrill AM, Reistad N (2016): Beyond velocity and acceleration: jerk, snap and higher derivatives. European Journal of Physics, 37(6).

Eliker K, Bouadi H, Haddad M (2016): Flight planning and guidance features for an UAV Flight Management Computer. In: Proceedings of 2016 IEEE 21st International Conference on Emerging Technologies and Factory Automation (ETFA), Berlin, Germany, September 06 – 09: 1 – 6.

Eurocontrol (2017): Who we are. www.eurocontrol.int/articles/who-we-are, (October 2017).

European Commission (2011): Report from the Commission to the European Parliament and the Council: Mid-term review of the European satellite radio navigation programmes. COM(2011) 5. Available at http://eur-lex.europa.eu/legal-content/EN/TXT/?uri=CELEX:52011DC0005.

European Commission (2017): Unmanned aircrafts. http://ec.europa.eu/growth/sectors/aeronautics/rpas_de, (October 2017).

European Union (2016): European GNSS (Galileo) Open Service Signal-In-Space Interface Control Document (OS SIS ICD). Issue 1.3, December. Available at: www.gsc-europa.eu/system/files/galileo_documents/Galileo-OS-SIS-ICD.pdf.

European Aviation Safety Agency (2017a): The Agency. www.easa.europa.eu/the-agency/the-agency, (October 2017).

References

European Aviation Safety Agency (2017b): Notice of Proposed Amendment 2017-05: Introduction of a regulatory framework for the operation of drones. Available at: www.easa.europa.eu/document-library/notices-of-proposed-amendment/npa-2017-05.

European GNSS Agency (2017a): EGNOS. Available at http://egnos-portal.gsa.europa.eu/, (August 2017).

European GNSS Agency (2017b): GNSS Market Report. Issue 5, May. Available at: www.gsa.europa.eu/system/files/reports/gnss_mr_2017.pdf.

European Space Agency (2009): EGNOS: European Geostationary Navigation Overlay Service: Europe's first contribution to satellite navigation BR-284. Available at www.egnos-pro.esa.int/Publications/ESA_EGNOS_br284_2009.pdf.

Falcone M, Hahn J, Burger T (2017): Galileo. In: Teunissen PJ, Montenbruck O (eds.), Springer Handbook of Global Navigation Satellite Systems, 1st edition, Springer International Publishing, vol. 182 of Springer Handbooks.

Gupta SG, Ghonge MM, Jawandhiya PM (2013): Review of Unmanned Aircraft System (UAS). International Journal of Advanced Research in Computer Engineering & Technology, 2(4): 1646 – 1658.

Güttel I (2017): Technik-Test: Drohnen sollen bald auch außer Sichtweite fliegen. Aero International.de. Available at: www.aerointernational.de/aviation/43818.html, (09 October 2017).

Hern A (2016): Amazon claims first successful Prime Air drone delivery. The Guardian. Available at www.theguardian.com/technology/2016/dec/14/amazon-claims-first-successful-prime-air-drone-delivery, (14 December 2016).

References

Hofmann-Wellenhof B, Legat K, Wieser M (2003): Navigation – Principles of Positioning and Guidance. Springer, Wien New York.

Hofmann-Wellenhof B, Lichtenegger H, Collins J (2001): GPS – Theory and Practice, 5th edition. Springer, Wien New York.

Hofmann-Wellenhof B, Lichtenegger H, Wasle E (2008): GNSS – Global Navigation Satellite Systems: GPS, GLONASS, Galileo & more. Springer, Wien New York.

Hofmann-Wellenhof B, Moritz H (2006): Physical Geodesy, 2nd edition. Springer, Wien New York.

Hota S, Ghose D (2010): Optimal path planning for an aerial vehicle in 3D space. In: Proceedings of 49th IEEE Conference on Decision and Control (CDC), Atlanta, Georgia, December 15 – 17: 4902 – 4907.

International Civil Aviation Organization (2006): PANS-OPS: Procedures for Navigation Services – Aircraft Operations. DOC 8168, 5th edition.

International Civil Aviation Organization (2011): Unmanned Aircraft Systems (UAS). Cir 328 AN/190. Available at: `www.icao.int/Meetings/UAS/Documents/Circular%20328_en.pdf`.

International Civil Aviation Organization (2015): Manual on Remotely Piloted Aircraft Systems (RPAS). DOC 10019, 1st edition.

International Civil Aviation Organization (2017): About ICAO. `www.icao.int/about-icao/`, (October 2017).

Kalman RE (1960): A new approach to linear filtering and prediction problems. Journal of basic Engineering, 82(1): 35 – 45.

References

Kaplan ED, Leva JL, Milbert D, Pavloff MS (2006): Fundamentals of Satellite Navigation. In: Kaplan ED, Hegarty CJ (eds.), Understanding GPS: Principles and Applications, 2nd edition, Artech House, Norwood.

Kneissel F, Stöber C (2010): Combined Integrity of GPS and Galileo. InsideGNSS, 5(1): 52 – 63.

Koppert A (2015): GNSS-gestützte kooperative Kollisionserkennung für Fahrzeuge. Master thesis, Institute of Geodesy, Graz University of Technology, Austria.

Lin CE, Dimpudus KK, Hsu YC (2017): Airspace risk assessment in logistic path planning for UAV. In: Proceedings of 2017 Integrated Communications, Navigation and Surveillance Conference (ICNS), Herndon, Virgina, April 18 – 20: 6A1–1 – 6A1–9.

Lossau N (2017): Diese Spezialdrohne jagt bald Einbrecher. Welt N24. Available at `www.welt.de/wissenschaft/article161874755/Diese-Spezialdrohne-jagt-bald-Einbrecher.html`, (07 February 2017).

Misra P, Enge P (2001): Global Positioning System: Signals, Measurements, and Performance, 2nd edition. Ganga-Jamnua, Lincoln.

Osborne J, Rysdyk R (2005): Waypoint Guidance for Small UAVs in Wind. In: AIAA Infotech@ Aerospace, 193(1–4): 1 – 12.

Perrottet J (2017): Enabling unrestricted UAS airspace access: Performance based navigation. In: Proceedings of 2017 Integrated Communications, Navigation and Surveillance Conference (ICNS), Herdon, Virginia, April 18 – 20: 6D1–1 – 6D1–5.

Polychronopoulos A, Tsogas M, Amditis AJ, Andreone L (2007): Sensor Fusion for Predicting Vehicles' Path for Collision Avoidance Systems. IEEE Transactions on Intelligent Transportation Systems, 8(3): 549 – 562.

References

Radio Technical Commission for Aeronautics (1999): Minimum Operational Performance Standards for Global Positioning System / Wide Area Augmentation System Airborne Equipment. DO-229B, Special Committee no. 159, Washington DC.

Salzburger Nachrichten (2017): Drohne kam Hubschrauber in Salzburg gefährlich nahe. Available at `www.sn.at/salzburg/chronik/drohne-kam-hubschrauber-in-salzburg-gefaehrlich-nahe-11966107`, (08 June 2017).

SESAR Joint Untertaking (2016): European Drones Outlook Study – Unlocking the value for Europe. Available at: `www.sesarju.eu/sites/default/files/documents/reports/European_Drones_Outlook_Study_2016.pdf`.

SESAR Joint Untertaking (2017): U-space (Blueprint). Available at `www.sesarju.eu/u-space-blueprint`.

Shau-Shiun J (2002): Analysis of a Three-Frequency GPS/WAAS Receiver to Land an Airplane. In: Proceedings of ION GPS 2002, 15$^{\text{th}}$ International Meeting of the Satellite Division of the Institute of Navigation, Portland, Oregon, September 24 – 27: 2576 – 2586.

Skinnemoen H (2014): UAV & satellite communications live mission-critical visual data. In: Proceedings of 2014 IEEE International Conference on Aerospace Electronics and Remote Sensing Technology, Yogykarta, Indonesia, November 13 – 14: 12 – 19.

Soares Lira da Silva AL, de Carvalho Bertoli G, Tosta RP, Ribeiro MA, Adabo GJ (2016): Beyond line-of-sight UAS communication link simulation. In: Proceedings of 2016 International Conference on Unmanned Aircraft Systems (ICUAS), Arlington, Virginia, June 07 – 10: 135 – 143.

Sujit PB, Saripalli S, Sousa JB (2014): Unmanned Aerial Vehicle Path Following: A Survey

and Analysis of Algorithms for Fixed-Wing Unmanned Aerial Vehicles. IEEE Control Systems, 34(1): 42 – 59.

Torge W, Müller J (2012): Geodesy, 4th edition. De Gruyter textbook, Berlin, Boston: De Gruyter.

US Air Force (2017): GPS: Global Positioning System. `www.gps.gov`, (August 2017).

Ventura-Traveset J, López de Echazarreta C, Lam JP, Flament D (2015): An Introduction to EGNOS: The European Geostationary Navigation Overlay System. In: Nurmi J, Lohan ES, Sand S, Hurskainen H (eds.), GALILEO Positioning Technology, Springer, The Netherlands, vol. 182 of Signals and Communication Technology.

Walter T, Enge P, Hansen A (1997): A Proposed Integrity Equation for WAAS MOPS. In: Proceedings of ION GPS 1997, 10th International Technical Meeting of the Satellite Division of The Institute of Navigation, Kansas City, Missouri, September 16 – 19: 475 – 484.